Geo-Bio Interfaces (2025), **2**, e4, 1–17
doi:10.1180/gbi.2024.7

CAMBRIDGE UNIVERSITY PRESS

Article

Formation of amorphous molybdenum sulfide in abiotic and biotic sulfidic conditions: A comparative study on molybdenum sequestration mechanisms

Rachel F. Phillips[1,2], Weinan Leng[3], Sheryl A. Singerling[3,4], Morgane Desmau[5] and Jie Xu[1]

[1]School of Molecular Sciences, Arizona State University, Tempe, AZ, USA; [2]School of Earth, Ocean and Environment, University of South Carolina, Columbia, SC, USA; [3]The National Center for Earth and Environmental Nanotechnology Infrastructure, Virginia Tech, Blacksburg, VA, USA; [4]Schwiete Cosmochemistry Laboratory, Goethe University, Frankfurt, Germany and [5]Canadian Light Source, University of Saskatchewan, Saskatoon SK, Canada.

Abstract

Concentrations of sedimentary molybdenum (Mo) have been used as a proxy for palaeoceanographic redox conditions based on the distinctive behaviour of Mo under oxic versus euxinic (*i.e.*, anoxic and sulfidic) conditions. However, the mechanisms that govern Mo sequestration in various euxinic settings are not fully resolved. It has previously been proposed that sulfate-reducing bacteria (SRB), the main drivers and regulators of euxinic conditions, can actively take up and reduce Mo intracellularly and passively induce Fe-independent Mo complexation and reduction at their cell surfaces. However, uncertainties remain regarding the underlying interactions and relative contributions of these proposed biotic Mo sequestration pathways. In this study, systematic experiments were carried out to examine the interactions among Mo(VI) species (MoO_4^{2-} or MoS_4^{2-}), ferrous iron (Fe^{2+}) and SRB with a focus on combinations of conditions that lead to reductive Mo precipitation. The speciation of aqueous Mo and composition, structure, oxidation states and bonding environment of precipitated Mo-sulfides were analysed using UV-vis spectrophotometry (UV-vis), transmission electron microscopy (TEM), X-ray photoelectron spectroscopy (XPS) and synchrotron-based X-ray absorption spectroscopy (XAS). Results indicate that SRB does not directly reduce Mo but, rather, plays a passive role in mediating Mo sequestration by providing sulfide and potential nucleation sites at their reactive cell surfaces for precipitation. However, even in the presence of SRB cells, Fe^{2+} was required for Mo precipitation in all conditions tested. By identifying the limiting (and non-limiting) factors in the Mo reduction and sequestration process, this study provides significant new insights for interpreting Mo palaeoredox proxies.

Keywords: Paleoredox proxy; Molybdenum sequestration; Sulfate-reducing bacteria; Molybdenum sulfides; Molybdate; Thiomolybdate

(Received 12 June 2024; revised 01 October 2024; manuscript accepted: 24 October 2024)

Highlights

- Mo sequestration is driven by abiotic processes and only indirectly facilitated by sulfate-reducing bacteria (SRB) through their production of sulfide
- Mo sequestration is Fe-dependent in both abiotic and biotic (SRB-containing) solutions at circumneutral pH.
- Mo precipitates formed under abiotic and biotic conditions are analytically indistinguishable.

Introduction

Molybdenum (Mo), the most abundant trace metal in modern oceans, remains predominantly dissolved as the oxyanion molybdate (MoO_4^{2-}) in oxic water, whereas, in euxinic (*i.e.*, anoxic and sulfidic) conditions, it reacts with sulfide to form thiomolybdate ($MoO_xS_{4-x}^{2-}$), which eventually becomes reduced and sequestered into the sediment (Helz et al., 1996). Due to its redox sensitivity, Mo is widely used for reconstructing palaeoceanographic conditions (*e.g.*, Hlohowskyj et al., 2021). However, the underlying mechanisms that drive Mo sequestration under euxinic conditions remain poorly understood, specifically regarding the relative contribution of abiotic and biotic mechanisms. Because Mo is a bio-essential element, and strong correlations between organic matter (OM) and Mo in the rock record have been observed, it has been proposed that biological organisms and/or particulate OM play important roles in Mo complexation and sequestration in euxinic basins (*e.g.*, Tribovillard et al., 2004; Algeo and Lyons, 2006; Mendel and Bittner, 2006; Lyons et al., 2009; Chappaz et al., 2014; Dahl et al., 2017; Wagner et al., 2017; Dellwig et al., 2019).

Studies investigating Mo removal via OM complexation under euxinic conditions have focused on the role of sulfate-reducing bacteria (SRB) cells as bacterial sulfate reduction is the main input of sulfide in euxinic settings (*e.g.*, Jørgensen and Kasten, 2006;

Corresponding authors: Rachel F. Phillips and Jie Xu Emails: rp66@mailbox.sc.edu; jiexu10@asu.edu

Cite this article: Phillips R.F., Leng W., Singerling S.A., Desmau M., & Xu J. (2025). Formation of amorphous molybdenum sulfide in abiotic and biotic sulfidic conditions: A comparative study on molybdenum sequestration mechanisms. *Geo-Bio Interfaces* **2**, e4, 1–17. https://doi.org/10.1180/gbi.2024.7

Jørgensen et al., 2019). In most scenarios, euxinia development is closely tied to OM burial and preservation (Scott et al., 2017). While it has been shown that under abiotic sulfidic conditions at circumneutral to high pH the presence of ferrous iron (Fe^{2+}) is required for Mo reduction and sequestration (Phillips et al., 2023), evidence for Mo-sulfide precipitation in the presence of live or dead SRB cells suggests an iron-independent pathway of Mo sequestration (Dahl et al., 2017). However, the role of iron as a prerequisite for Mo sequestration and the mechanisms behind a potential iron-independent biological pathway remain poorly understood.

Although SRB is known to transport MoO_4^{2-} into their cells as it is a structural analogue to their typical electron acceptor, sulfate (SO_4^{2-}) (Stoeva and Coates, 2019), it is unclear if or how the Mo(VI) in MoO_4^{2-} becomes reduced to Mo(IV) once inside the cell. Molybdenum is necessary for the biosynthesis and function of many enzymes, including dimethylsulfoxide (DMSO) reductase, which is a type of molybdoenzyme found in nitrate-reducing bacteria as well as some SRB species (Jonkers et al., 1996; Tucker et al., 1997; Tucker et al., 1998; Wichard et al., 2009; Crichton, 2019; Demtröder et al., 2019). Thus, Mo could be used for enzyme production by SRB once transported intracellularly, which could subsequently lead to its reduction via intracellular organic ligands and sequestration upon OM degradation (Orberger et al., 2007). Similarities between structures of Mo species in euxinic sediment and specific molybdoenzyme structures (Dahl et al., 2017) have fueled hypotheses of such biologically mediated Mo sequestration pathways. It has also been proposed that Mo can be reduced and sequestered upon interaction with periplasmic proteins containing intermediate sulfur species formed during bacterial sulfate reduction (Chen et al., 1998). Such biological Mo sequestration mechanisms via SRB interactions are, however, contradictory because molybdate inhibits bacterial sulfate reduction – the main energy source for the bacteria (*e.g.*, Chen et al., 1998; Biswas et al., 2009; Stoeva and Coates, 2019), suggesting that SRB alone are unlikely to account for the abundance of Mo found in euxinic sediments. Rather than active uptake and metabolic reduction of Mo, SRB may employ extracellular enzymes targeted at immobilizing Mo for detoxification purposes (Hale et al., 2001; Phillips and Xu, 2021). Although the concentrations of Mo in natural euxinic environments may be insufficient to cause such a reaction by SRB (Mohajerin et al., 2016), where sulfate is deficient, Mo toxicity to SRB is enhanced leading to possible detoxification reactions and Mo reduction. In summary, all the proposed SRB-induced Mo sequestration pathways (*i.e.*, passive complexation, metabolic reduction and enzymatic immobilization and reduction) may contribute to the total Mo removed from natural euxinic basins.

Molybdenum in cell-associated precipitates formed via MoO_4^{2-}-SRB interactions has a similar bonding structure as the Mo species found in modern euxinic sediment (Dahl et al., 2013; Dahl et al., 2017), lending credence to the proposed biological sequestration pathways. However, it has also been suggested that the organic functional groups provided by SRB that complex and sequester Mo are probably not abundant enough in natural settings to account for a significant portion of Mo in euxinic sediment (Dellwig et al., 2007; Helz and Vorlicek, 2019). Therefore, the positive correlations between OM and Mo in the rock record may reflect the indirect rather than direct role of SRB, in which they produce sulfide with which Mo reacts, inducing its abiotic sequestration (Helz and Vorlicek, 2019). In this study, we experimentally investigated Mo-SRB interactions and associated Mo precipitates to provide new insights into the ongoing debate of whether the previously reported OM and Mo covariation in euxinic sediments resulted from direct Mo-OM/cell interactions or the indirect role of SRB via sulfide production. We conducted a range of experiments involving Mo (as either MoO_4^{2-} or MoS_4^{2-}), Fe^{2+} and SRB cells. The findings from this investigation emphasize the importance of Fe-dependent pathways of Mo sequestration over OM and biologically facilitated pathways and illuminate the molecular interactions and precipitation mechanisms involved in such pathways.

Methods

Biological experiments were carried out to examine the effect of live and dead SRB cells on dissolved Mo speciation, reduction, sequestration, precipitation composition and structure. Two different species of SRB were used in these experiments, *Desulfovibrio vulgaris* and *Desulfotignum balticum*, to increase the environmental relevancy of the experiments as these species are isolates of different euxinic niches and grow optimally at distinct salinities (*D. vulgaris* in brackish solutions at an ionic strength of ~ 0.1 M and *D. balticum* in saline marine conditions at an ionic strength of ~ 0.7 M; Table S1). Pure cultures of *D. vulgaris* and *D. balticum* were prepared in anaerobic salt-water media (Table S1). After the addition of the media ingredients to MQ water (18.2 MΩ·cm), each medium was degassed for 20 minutes with nitrogen gas (N_2) and the pH was adjusted using NaOH. The media were then separated into serum vials, each containing 100 ml of media solution, degassed for another 40 minutes, sealed with butyl rubber stoppers and autoclaved for 15 minutes at 121°C. Once sterile, SRB species were inoculated into their respective media. The final post-autoclaving, pre-inoculation pH of *D. vulgaris* media averaged 6.67 ± 0.14 and that of *D. vulgaris* media averaged 7.32 ± 0.11.

Experiments containing 0.5 mM Mo, 5 mM sulfide and various concentrations of Fe (ranging from 0 to 1 mM) were carried out in inoculated (SRB-containing) and uninoculated (abiotic) media solutions to allow comparison of Mo behaviour in biotic and abiotic conditions. Molybdenum, iron and sulfide stock solutions were prepared for the addition of such species into bacterial cultures using reagents purchased from Sigma Aldrich of ACS grade or higher, including $Na_2S{\cdot}9H_2O$ (for abiotic experiments), molybdate ($Na_2MoO_4{\cdot}2H_2O$), tetrathiomolybdate (NH_4MoS_4) and ferrous iron (*i.e.*, $Fe(II)Cl_2$). Previous studies pointed out the potential for Mo(V) contamination in commercial $(NH_4)_2MoS_4$ (Chandrasekaran et al., 1987; Vorlicek et al., 2018; Phillips et al., 2023). Thus, in all experiments for which the oxidation state of Mo in the final precipitate was measured, $Na_2MoO_4{\cdot}2H_2O$ was used as the initial source of (thio) molybdate by reacting it with sulfide, tracking its speciation via UV-visible spectrophotometry (see section on UV-vis below) and timing the addition of Fe accordingly. Sample vials remained sealed throughout the duration of each experiment and all additions of Mo, Fe and/or S from stock to culture solutions were carried out via sterilized syringes and needles inside an anaerobic chamber under an N_2:H_2 = 97%:3% atmosphere.

SRB growth in the presence of Mo

One set of cultures was grown in Mo-containing media to test the toxicity of Mo toward SRB and assess the differences (if any) between the effects of molybdate (MoO_4^{2-}) and tetrathiomolybdate (MoS_4^{2-}) on SRB growth. In these experiments, 0.5 mM Mo (either as MoO_4^{2-} or MoS_4^{2-}) was added to the media prior to bacterial inoculation. These experiments were carried out in the presence and absence of Fe^{2+} to determine whether Fe^{2+} is required for Mo sequestration in

https://doi.org/10.1180/gbi.2024.7 Published online by Cambridge University Press

the presence of SRB, as it has been shown to be required in the absence of bacteria (Phillips et al., 2023). In the Fe^{2+}-containing cultures, Fe^{2+} was added to the media prior to inoculation and after ageing to allow thorough Mo-SRB cell culture interactions before Fe^{2+} addition.

SRB growth in the absence of Mo

A second set of SRB cell cultures was initially grown in the absence of Mo or Fe^{2+} until a sulfide concentration of ~5 mM was reached. Sulfide concentrations in the SRB cell culture solutions were monitored using a spectrophotometric assay (Xu et al., 2016) against a 10-point calibration curve made with solutions of known sulfide concentrations with a similar composition to that of the samples. Once 5 mM sulfide was produced in the SRB cell cultures, Mo and Fe^{2+} were added to induce FeMoS precipitation. A sulfide concentration of 5 mM was targeted to create conditions comparable to the parallel uninoculated/abiotic experiments, which were carried out at 5 mM sulfide. This set of experiments was also carried out in both the presence and absence of ferrous iron. In the Fe-containing experiments, cultures were inoculated with 0.5 mM of both Mo (as MoO_4^{2-}) and Fe^{2+} once 5 mM of sulfide was produced. In the Fe-lacking experiments, cultures were inoculated with 0.5 mM of Mo (as MoO_4^{2-}) only once 5 mM of sulfide was produced. These experiments were only conducted using MoO_4^{2-} rather than MoS_4^{2-} because enough sulfide had been produced by the SRB by the time of Mo addition that the MoO_4^{2-} would become fully thiolated (converted to MoS_4^{2-}) throughout the experimental duration.

Dead SRB cell experiments

In another set of cultures, SRB was grown in the absence of Fe^{2+} and Mo and killed via autoclave before the addition of the metals. Similar to the set of live experiments explained previously, sulfide concentrations of these cultures were monitored using a spectrophotometric assay as the SRB grew. Once 5 mM sulfide was produced, the SRB were killed and 0.5 mM Fe^{2+} and Mo (as MoO_4^{2-}) were added to the dead cell-containing solutions to assess the effect of dead SRB cells on the speciation and sequestration of molybdenum. This set of experiments was also tested in both Fe-containing and Fe-lacking solutions to determine whether the presence of dead SRB cells allows for Fe-independent Mo sequestration, as has been previously proposed (Dahl et al., 2017).

Table 1. XANES LCF vs XPS Mo oxidation state data.

Sample	Exp. Duration	Initial Fe: Mo_{aq}[a]	Initial pH[b]	Ionic Strength (M)	Final pH[c]	Mo Oxidation State (XAS)	Mo Oxidation State (XPS)
Abiotic FeMoS experiments (from low to high pH)	40+ d	1.00	4.34	0.01	4.33	4.50	4.11
	40+ d	1.00	7.57	0.01	7.73	4.36	4.19
	40+ d	1.00	10.96	0.01	10.96	6.00	*not enough Mo*
Dv-L[e] (Fe+Mo added before inoc.)	~30 d	1.00	6.71[e]	0.1	6.88	–	4.22
Dv-L (Fe added before inoc.)	~30 d	1.00	6.65[e]	0.1	6.94	–	–
Dv-L (Mo added before inoc.)	~30 d	1.00	6.67[e]	0.1	7.01	–	4.15
Dv-L (TM added before inoc.)	~30 d	1.00	6.70[e]	0.1	7.03	–	–
Dv-D (Fe+Mo added to dead cell culture)	~30 d	1.00	6.71[e]	0.1	6.89	–	4.20
Db-L (Fe+Mo added before inoc.)	~30 d	1.00	7.38[e]	0.7	7.45	–	–
Db-L (Fe added before inoc.)	~30 d	1.00	7.33[e]	0.7	7.48	–	4.16
Db-L (Mo added before inoc.)	~30 d	1.00	7.35[e]	0.7	7.39	–	–
Db-L (TM added before inoc.)	~30 d	1.00	7.38[e]	0.7	7.56	–	–
Db-D (Fe+Mo added to dead cell culture)	~30 d	1.00	7.36[e]	0.7	7.49	–	–
Time Series: Live *D. vulgaris* cultures	5 min	1.00	6.85	0.1	7.01	4.34	4.81
	3 h	1.00	6.78	0.1	6.99	–	4.49
	24 h	1.00	6.89	0.1	7.00	4.16	4.16
	4 d	1.00	6.80	0.1	7.12	4.38	–
	8 d	1.00	6.82	0.1	7.19	4.16	4.26
	40+ d	1.00	6.91	0.1	7.32	4.00	4.17
Time Series: Uninoculated *D. vulgaris* media	5 min	1.00	7.16	0.1	7.19	4.38	4.25
	3 h	1.00	7.17	0.1	7.18	–	4.12
	24 h	1.00	7.16	0.1	7.22	4.42	4.15
	4 d	1.00	7.20	0.1	7.29	4.36	–
	8 d	1.00	7.18	0.1	7.42	4.44	4.18
	40+ d	1.00	7.19	0.1	7.56	4.25	4.18

(*Continued*)

https://doi.org/10.1180/gbi.2024.7 Published online by Cambridge University Press

Table 1. (*Continued*)

Sample	Exp. Duration	Initial Fe: Mo_{aq}[a]	Initial pH[b]	Ionic Strength (M)	Final pH[c]	Mo Oxidation State (XAS)	Mo Oxidation State (XPS)
[Fe] Series: Live *D. vulgaris* cultures	160+ d	~0.03[d]	6.81	0.1	7.12	–	4.30
	40+ d	0.50	6.88	0.1	7.36	4.40	4.19
	40+ d	1.00	6.91	0.1	7.32	4.00	4.17
	40+ d	2.00	6.82	0.1	7.29	4.36	4.15
[Fe] Series: Uninoculated *D. vulgaris* media	80+d	0.02	7.20	0.1	7.29	–	4.71
	80+d	0.10	7.31	0.1	7.40	–	4.74
	40+ d	0.50	7.17	0.1	7.23	–	4.13
	40+ d	1.00	7.19	0.1	7.56	4.25	4.18
	40+ d	2.00	7.12	0.1	7.14	4.40	4.25
[Fe] Series: Live *D. balticum* cultures	160+ d	~0.03[d]	7.75	0.7	8.31	–	–
	80+ d	0.50	7.57	0.7	7.76	–	4.42
	80+ d	1.00	7.55	0.7	7.69	–	4.21
	80+ d	2.00	7.56	0.7	7.79	–	4.39
[Fe] Series: Uninoculated *D. balticum* media	80+ d	0.50	7.89	0.7	7.92	–	4.14
	80+ d	1.00	7.92	0.7	7.99	4.34	4.17
	80+ d	2.00	7.88	0.7	7.97	–	4.15

[a]Initial Fe:Mo was altered by changing initial [Fe] (from 0.01 to 0.5 mM). Initial [Mo] remained 0.5 mM in all experiments.
[b]Initial pH was taken after autoclaving and 5mM sulfide addition/production.
[c]Final pH was taken from supernatant after aging (i.e., experimental duration).
[d]These experiments were initially meant to contain no Fe, but a small amount of Fe was transferred during inoculation of the media (see the discussion section on Mo thiolation in abiotic and biotic systems).
[e]Initial pH for these experiments was taken before inoculation/sulfide production via SRB growth.

Monitoring sample solutions with ultraviolet-visible spectroscopy (UV-vis)

Bacterial growth, sulfide production and dissolved Mo speciation were monitored in sample solutions using UV-vis over the course of ageing (which ranged from 5 minutes to ~4000 hours, or ~160 days, depending on the sample; Table 1). Molybdate thiolation (conversion of molybdate to tetrathiomolybdate via reaction with sulfide: $MoO_4^{2-} \rightarrow MoS_4^{2-}$) is a stepwise process that involves the formation of three thiomolybdate intermediate species (MoO_3S^{2-}, $MoO_2S_2^{2-}$ and $MoOS_3^{2-}$) before the final product, tetrathiomolybdate (MoS_4^{2-}), forms. Because each dissolved thiomolybdate species has distinct absorption characteristics, UV-vis was used to track the presence, type and relative abundances of thiomolybdate species in the experimental solutions throughout ageing to determine the effect of SRB on the rate and degree of Mo thiolation. All UV-vis absorption spectra were obtained for a wavelength range of ~275 – 500 nm, given that all thiomolybdate absorbance peaks are within this range (Erickson and Helz, 2000; Dahl et al., 2017). It should be noted that 'full thiolation' as discussed in the results and discussion refers to solutions in which molybdate was converted to tetrathiomolybdate as indicated by characteristic peaks in the UV-vis spectra of the samples. That said, the presence of tetrathiomolybdate peaks in the UV-vis spectra, even if peaks characteristic of other thiomolybdate species are absent, does not mean the solution contains only tetrathiomolybdate. Thermodynamic and reaction kinetic considerations suggest that our solutions dominated by tetrathiomolybdate (MoS_4^{2-}) probably also contained di- and trithiomolybdate species ($MoO_2S_2^{2-}$ and $MoOS_3^{2-}$) in amounts that could not be resolved using UV-vis (Vorlicek et al., 2015; Hlohowskyj et al., 2021). After ageing, precipitates were separated and analysed by XPS and TEM for Mo oxidation state, speciation and structure. Sample preparation methods for each technique are described in the following sections.

X-ray spectroscopy and transmission electron microscopy

Precipitates were analysed by X-ray photoelectron spectroscopy (XPS), X-ray absorption spectroscopy (XAS) and transmission electron microscopy (TEM) to determine the elemental concentrations and oxidation states, as well as the Mo bonding environment and overall structure of the FeMoS precipitates. After ageing, samples were prepared for XPS, XAS and TEM in an anaerobic chamber (N_2:H_2 = 97%:3%) via centrifugation, separation, sonication and washing steps outlined in Phillips et al. (2023). The isolated precipitates were dried and ground into fine powder using a mortar and pestle for XPS and XAS specimen preparation.

The powdered samples were separated into two parts for XPS and XAS analyses. The XPS analyses were conducted on a PHI Quantera SXM at the Nanoscale Characterization and Fabrication Laboratory at Virginia Tech, with a monochromatic X-ray source (Al *Kα*: 1486.6 eV) for small-spot analysis. The Multipak software was used to fit the high-resolution XPS spectra. Charge correction was done using the C 1s peak at 284.8 eV. Details regarding parameters used for peak fitting of high-resolution Mo, Fe and S XPS spectra are discussed in the supplementary information (SI) file. For XAS, the powdered samples were spread in between two pieces of Kapton Tape and analysed on the BioXAS-Main

https://doi.org/10.1180/gbi.2024.7 Published online by Cambridge University Press

spectroscopy beamline at the Canadian Light Source (CLS) facility at the University of Saskatchewan. Details regarding Mo K-edge XANES analyses, XANES linear combination fitting (LCF) parameters, EXAFS analyses and EXAFS fitting parameters are included in the supplementary information file.

For TEM, samples were prepared on gold TEM grids with thin carbon support films and analysed at the Nanoscale Characterization and Fabrication Laboratory at Virginia Polytechnic Institute and State University on a JEOL JEM 2100 S/TEM, operated at 200 kV. TEM bright field images were taken with a Gatan Ultrascan 1000XP CCD camera, selected area electron diffraction (SAED) patterns were obtained on a Gatan Orius 833 slow scan CCD camera and energy dispersive X-ray spectroscopy (EDS) data were collected using a JEOL genuine 60 mm^2 Silicon Drift Detector in scanning TEM (STEM) mode. For transport, XPS, XAS and TEM samples were packed in sealed bags that were then placed in airtight Thermo Scientific AnaeroPack containers with oxygen scavengers before removal from the anaerobic chamber.

Inductively coupled plasma - optical emission spectroscopy (ICP-OES)

Sample supernatants removed during XAS, XPS and TEM sample preparation were saved and analysed via ICP-OES to obtain final aqueous Mo and Fe concentrations after ageing. Supernatant solutions were filtered through 0.2 µm syringe filters and acid digested to a final concentration of 2% HNO_3 in preparation for ICP-OES analyses, which were performed on an Agilent 5900 Synchronous Vertical Dual View (SVDV) ICP-OES at Arizona State University Core Research Facilities.

Results

SRB growth in Mo-containing media

When MoO_4^{2-} was added to *D. vulgaris* and *D. balticum* media before inoculation of bacteria, the growth (measured as the rate and total amount of sulfide production) of either SRB species was significantly reduced (Fig. S1). When MoS_4^{2-} was added to *D. vulgaris* and *D. balticum* media before inoculation, a similar inhibiting effect was observed, but sulfide concentrations were more variable due to the precipitation of Mo-sulfides.

In the MoO_4^{2-}-containing media (at ~0.5 mM Mo), *D. vulgaris* only produced about ~2.4% (by weight) of the sulfide produced in their Mo-free counterpart. These cultures were observed for over a year and there was no further growth. In the MoO_4^{2-}-containing media (at ~0.5 mM Mo), *D. balticum* produced about ~3.1% (by wt.) of the sulfide produced in their Mo-free counterpart. Similarly, in the MoS_4^{2-}-containing media (at ~0.5 mM Mo), *D. vulgaris* produced about ~1.8% (by wt.) of the sulfide produced in their Mo-free counterpart and *D. balticum* produced about ~0.6% (by wt.) of the sulfide produced in the corresponding Mo-free media. It is noted that the amount of sulfide produced in the MoS_4^{2-}-containing cell cultures was more variable given that sulfide precipitation occurred concomitantly with SRB growth in these cultures.

When Fe^{2+} and MoO_4^{2-} were added before inoculation of *D. vulgaris*, Mo precipitation was negligible, even in cultures aged over one year, due to a lack of *D. vulgaris* growth and sulfide production in the presence of molybdenum. However, *D. balticum* cultures with Fe and Mo added before inoculation did eventually form black FeMoS precipitates. Thus, although the *D. balticum* growth was slower in the presence of MoO_4^{2-}, it was not as strongly inhibited as that of *D. vulgaris*.

Mo thiolation and sequestration in abiotic and biotic systems

Molybdate thiolation was monitored using UV-vis for live SRB cultures, uninoculated SRB media and abiotic solutions with no culture media constituents (Table S1). To keep the sulfide concentrations consistent across samples, molybdate was added to live SRB cultures after ~5 mM sulfide was produced because 5 mM sulfide concentrations were used in abiotic and uninoculated systems. Molybdate was converted to tetrathiomolybdate in all live *D. vulgaris* and *D. balticum* cultures, as well as uninoculated media,

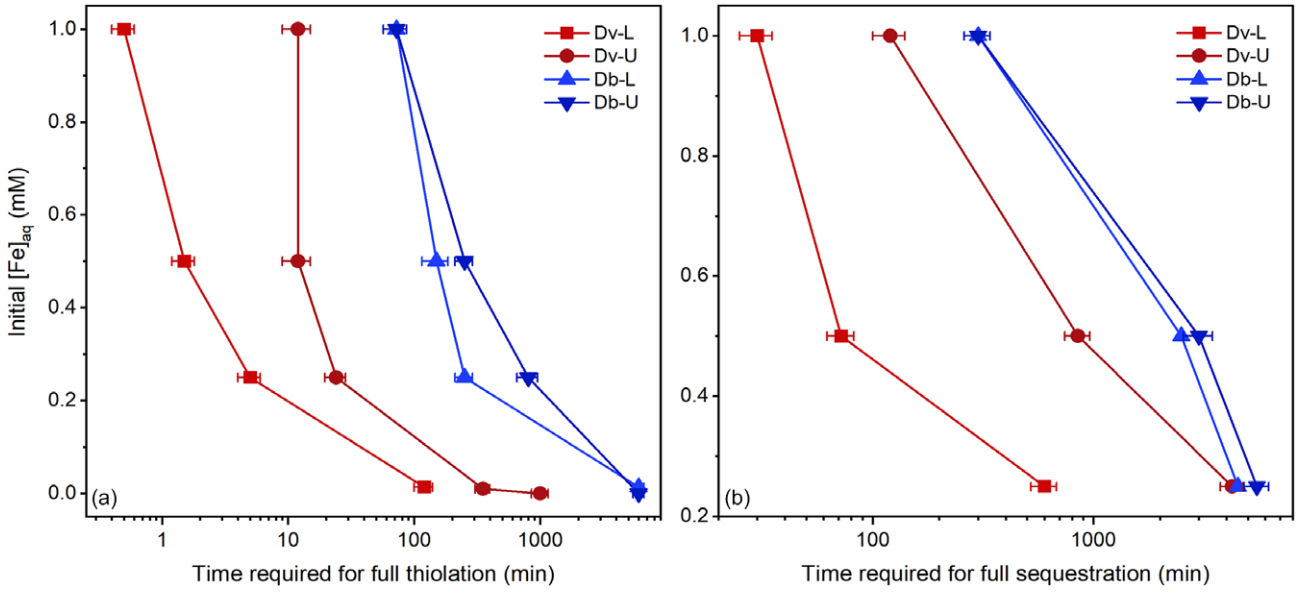

Figure 1. (a) Time required for full Mo thiolation (i.e., the time required for conversion of MoO_4^{2-} into MoS_4^{2-} as indicated by the presence of MoS_4^{2-} peaks and absence of thiomolybdate intermediate peaks in UV-vis spectra). (b) Time required for full Mo sequestration (i.e., as indicated by the absence of all $MoO_xS_{4-x}^{2-}$ peaks in UV-vis spectra) in live (L) and uninoculated (U) *D. vulgaris* (Dv) and *D. balticum* (Db) media.

https://doi.org/10.1180/gbi.2024.7 Published online by Cambridge University Press

but Mo thiolation occurred at different rates in each system depending mainly on pH and Fe^{2+} concentration (Fig. S2). At circumneutral pH and in the absence of Fe^{2+}, full Mo thiolation (*i.e.*, conversion of molybdate to tetrathiomolybdate, as indicated by UV-vis speciation; see methodology section on UV-vis for details) occurred ~8× faster in live *D. vulgaris* cultures compared to uninoculated *D. vulgaris* media, whereas, in *D. balticum* solutions, Mo thiolation rates in live cultures were relatively similar to that in uninoculated media (Fig. 1a).

In the presence of Fe^{2+}, and with increasing Fe^{2+} concentrations, Mo thiolation rates increased across all abiotic and biotic samples (Fig. 1). At circumneutral pH and an initial Fe:Mo ratio of 1:2, full Mo thiolation occurred ~5× faster in live *D. vulgaris* cultures than in uninoculated *D. vulgaris* media, whereas Mo thiolation rates were only ~3× faster in live *D. balticum* cultures than in uninoculated *D. balticum* media (Fig. 1a; Table S2). At an initial Fe:Mo ratio of 1:1, full Mo thiolation occurred ~8× faster in live *D. vulgaris* cultures than in uninoculated *D. vulgaris* media, whereas Mo thiolation rates were only ~2× faster in live *D. balticum* cultures than in uninoculated *D. balticum* media (Fig. 1a). At an initial Fe:Mo ratio of 2:1, full Mo thiolation occurred ~24× faster in live *D. vulgaris* cultures than in uninoculated *D. vulgaris* media, whereas Mo thiolation rates were roughly the same in live and uninoculated *D. balticum* solutions (Fig. 1a). In all conditions tested, Mo thiolation was consistently faster in *D. vulgaris* media compared to *D. balticum* media (Fig. 1a).

The presence of Fe^{2+} also induced Mo sequestration via FeMoS precipitation. Complete Mo sequestration (measured by the absence of molybdate or thiomolybdate peaks in UV-vis spectra and corroborated with ICP-OES time series data) occurred ~8, 12 and 4× faster in live *D. vulgaris* cultures than in uninoculated *D. vulgaris* media at initial Fe:Mo ratios 1:2, 1:1 and 2:1, respectively (Fig. 1b). It should be noted that 'complete Mo sequestration' here refers the point at which aqueous Mo concentrations go below the detection limit of UV-vis; thus, Mo is not completely removed from solution. In fully aged media solutions (both uninoculated and inoculated *D. vulgaris* and *D. balticum* media) at an initial Fe:Mo ratio of 1:1, final aqueous Mo concentrations were 0.0001 – 0.06 mM (Table S3) based on ICP-OES analyses. For *D. balticum*, complete Mo sequestration was not reached in live or uninoculated samples within the ~200-day ageing period at an initial Fe:Mo ratio of 1:2. At initial Fe:Mo ratios of 1:1 and 2:1, complete Mo sequestration was reached within a similar timeframe in both live and uninoculated *D. balticum* samples (Fig. 1b).

The catalysing effect of Fe^{2+} on Mo thiolation and sequestration was observed for all conditions tested and remained relatively constant with changes in pH, ionic strength, presence of SRB cells and species of SRB (Fig. 1). Molybdenum sequestration appears to be even more strongly catalysed by the presence of Fe^{2+} compared to Mo thiolation. With every additional 0.5 mM Fe^{2+} in *D. vulgaris* solutions, full Mo thiolation occurred 1–2× faster in uninoculated media versus ~3× faster in live cultures (Fig. 1a), whereas complete Mo sequestration occurred 5–7× faster in uninoculated media versus 2–8× faster in live cultures (Fig. 1b). With every additional 0.5 mM Fe^{2+} in *D. balticum* samples, full Mo thiolation occurred ~3× faster in uninoculated media versus ~2× faster in live cultures with every additional 0.5 mM Fe^{2+} (Fig. 1a), complete Mo sequestration occurred ~12× faster in uninoculated media versus ~10× faster in live cultures (Fig. 1b).

ICP-OES results

The final aqueous Mo concentrations, based on ICP-OES analyses, were lower in the experiments run with live SRB cells (0.0002 – 0.0111 mM at 1:1 initial Fe:Mo_{aq}) than those carried out in the absence of SRB (0.0233 – 0.0564 mM at 1:1 initial Fe:Mo_{aq}; Table S3). A consistent decrease in final aqueous Mo concentrations (*i.e.*, increased degree of Mo sequestration) is observed with increasing initial aqueous Fe^{2+} concentrations (Fig. 2a) and experimental duration (Fig. 2b). Figure 2a showcases a similar decreasing trend in aqueous Mo concentrations with increasing aqueous Fe concentrations from euxinic basins (Helz, 2021; Phillips et al., 2023, and references therein); however, it should be noted that the concentrations of Mo and Fe in these natural systems are much lower than their experimental concentrations. A positive relationship is also observed between the final experimental aqueous Fe and Mo concentrations (Fig. 2c).

XPS results

As mentioned in the previous section, no precipitation occurred in the absence of Fe^{2+}, regardless of whether SRB was present or absent. Based on the XPS analyses, precipitates formed in the presence of Fe^{2+} and SRB cells contain Fe:Mo (atomic) ratios roughly the same as those formed in the absence of SRB cells (0.87 ± 0.36 and 0.88 ± 0.35, respectively; Table S3). The final Mo concentrations measured in the FeMoS precipitates increase with experimental duration (from ~5 min to 40 d; Fig. 2b). The concentrations of Mo, Fe and S in the final FeMoS precipitates were higher in the abiotic (uninoculated) samples relative to those in the biotic ones. However, the S/(Fe+Mo) (atomic) ratios in abiotic and biotic precipitates are analytically indistinguishable (2.28 ± 1.16 and 2.28 ± 0.55, respectively); thus, the difference in elemental concentrations is probably due to the relative increase in carbon and other organic components in the precipitates formed in the presence of cells. The final precipitate Fe and S concentrations increase with increasing precipitate Mo concentrations (Fig. 2d). The final precipitate Mo, Fe and S concentrations all increase with increasing experimental duration, with the exception of later time points (~100 to 1000 h) in the live SRB cell-containing experiments (Table S3), which is probably due to the relative increase in organic carbon produced in these solutions.

The best fits of high-resolution Mo XPS spectra obtained for the FeMoS formed in the biotic and abiotic experiments indicate that Mo(IV) is the dominant Mo species in the precipitates across all time points and initial Fe^{2+} concentrations (Fig. S3; Table S4). Thus, the reduction of Mo(VI) to Mo(IV) is confirmed in all experiments where precipitation was observed. The oxidation state of Mo averaged 4.17 ± 0.03 (1sd) for abiotic samples and 4.22 ± 0.08 (1sd) for biotic samples based on the XPS data (Table 1). There was a slight decrease in the average Mo oxidation state against experimental duration (Fig. 3a), but there was no apparent trend in the Mo oxidation state with changing final Fe:Mo ratio (Fig. 3b), or sulfur concentration (*i.e.*, total sulfide precipitation) (Fig. 3c).

The best fits of the high-resolution Fe XPS spectra indicate the presence of both ferrous (Fe^{2+}) and ferric (Fe^{3+}) iron in the FeMoS precipitates (Figs S4). Precipitates formed in biological solutions contain an average of 53.92 ± 4.98 atomic % (at.%) Fe(II); those prepared in abiotic solutions contain an average of 53.21 ± 3.86 at % Fe(II) (Table S4). The sulfur speciation was also similar for FeMoS precipitates formed in abiotic and biotic

https://doi.org/10.1180/gbi.2024.7 Published online by Cambridge University Press

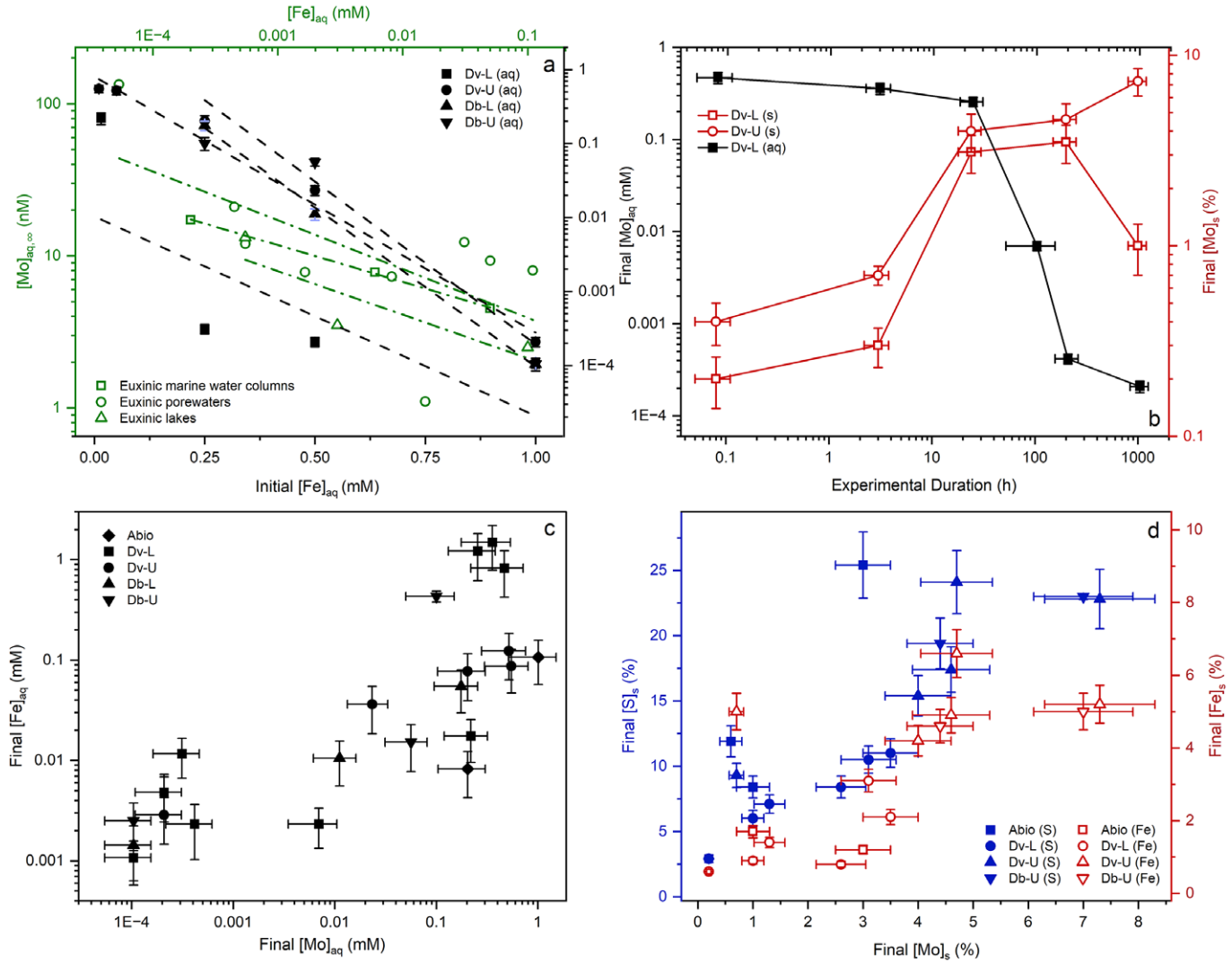

Figure 2. Trends in Mo, Fe, and S concentrations in solutions and solids: (a) final aqueous Mo concentrations ($[Mo]_{aq}$) against initial aqueous Fe concentrations ($[Fe]_{aq}$) compared to euxinic basin aqueous Mo data ($Mo_{aq,\infty}$) from Helz (2021) against aqueous Fe concentrations from the same basins ($[Fe]_{aq}$- top axis) from Phillips et al. (2023), and references therein (dashed lines are trendlines), (b) final $[Mo]_{aq}$ and final precipitate Mo concentration ($[Mo]_s$) against experimental duration, (c) final aqueous Fe concentrations ($[Fe]_{aq}$) against final $[Mo]_{aq}$, (d) final precipitate S and Fe concentrations ($[S]_s$ and $[Fe]_s$) against final $[Mo]_s$ and $[Mo]_{aq}$. Solid data is based on XPS and aqueous data is based on ICP-OES. Abio = abiotic solution with no media constituents; Dv/Db-L = live *D. vulgaris/D. balticum* cultures; Dv/Db-U = uninoculated *D. vulgaris/D. balticum* media.

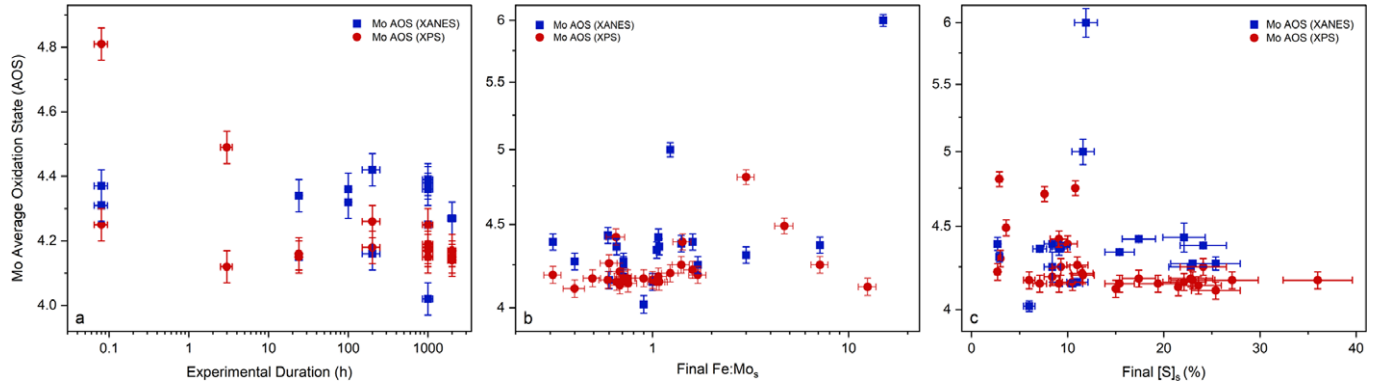

Figure 3. Average precipitate Mo oxidation state (XANES LCF & HR-XPS fitting data) against experimental duration (a), precipitate Fe:Mo ratios (b), and precipitate sulfur concentrations (c).

https://doi.org/10.1180/gbi.2024.7 Published online by Cambridge University Press

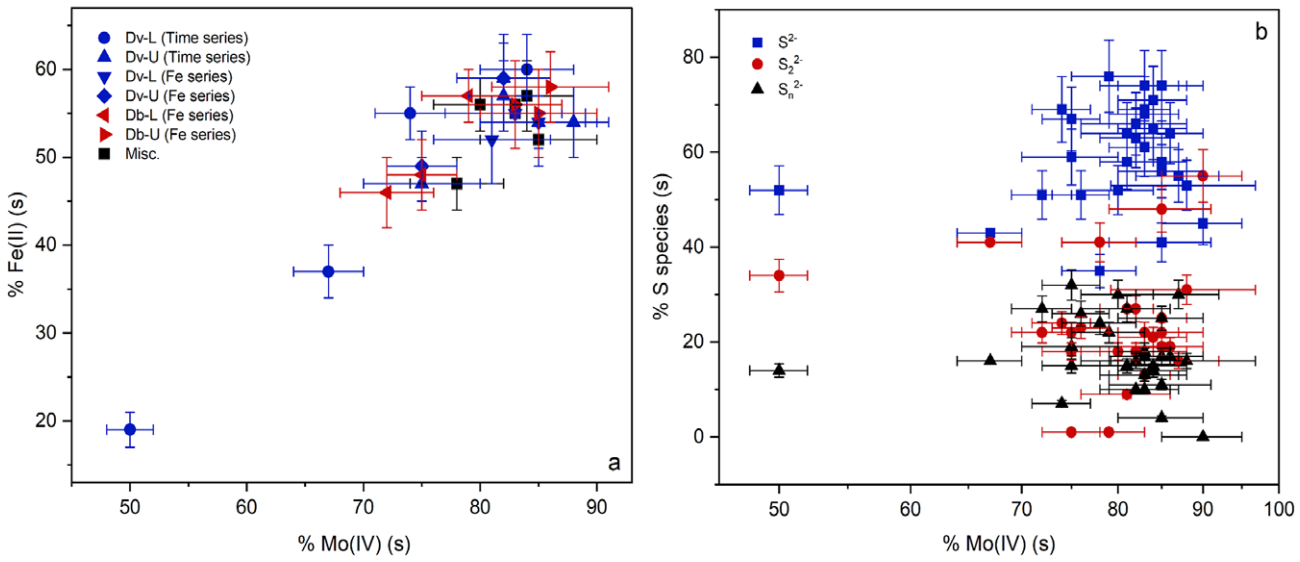

Figure 4. Percent reduced ferrous iron (Fe(II)) (a) and percent monosulfide (S^{2-}), disulfide (S_2^{2-}), and polysulfide (S_n^{2-}) (b) over percent reduced Mo(IV) in the FeMoS precipitates as calculated via HR-XPS fitting. Dv/Db-L = live *D. vulgaris/D. balticum* cultures; Dv/Db-U = uninoculated *D. vulgaris/D. balticum* media.

solutions (Figs S5), with an average of 63.14 ± 6.70 at.% monosulfide (S^{2-}), 20.36 ± 11.70 at.% disulfide (S_2^{2-}) and 16.57 ± 8.80 at.% polysulfide (S_n^{2-}) for abiotic samples, and 60.13 ± 12.50 at.% monosulfide (S^{2-}), 21.40 ± 11.18 at.% disulfide (S_2^{2-}) and 18.40 ± 6.55 at.% monosulfide (S_n^{2-}) for biotic samples (Table S5). There is a positive relationship between the degree of Mo reduction (percentage of Mo IV) and that of Fe (percentage of Fe II) in the precipitates (Fig. 4a). However, there is no apparent relationship between the degree of Mo reduction and sulfur speciation in the precipitates (Fig. 4b).

TEM results

The abiotic and biotic FeMoS precipitates analysed via TEM lack crystal structure based on selected area electron diffraction (SAED) analyses. The related EDS analyses semi-quantitatively constrained the Fe:Mo ratios in the precipitates (Table S5; Fig. S6). Abiotic and uninoculated samples have an average Fe:Mo ratio of 1.3 ± 0.9 (1sd). The Fe:Mo ratios in the precipitates formed in *D. vulgaris* or *D. balticum* cultures vary widely, averaging 7.1 ± 8.2 (1sd) and 7.7 ± 7.5 (1sd), respectively. When Fe^{2+} was added to the *D. vulgaris* culture before inoculation and Mo was added when SRB growth reached the exponential phase, the resulting precipitate contained a relatively high Fe:Mo ratio (22.7 ± 35.9). When Mo was added to cultures containing dead SRB cells, the Fe:Mo ratios in the resulting precipitates (7.84 ± 5.76 for *D. vulgaris* and 4.48 ± 0.00 for *D. balticum*) were within the range of those observed for precipitates formed in live SRB cultures (6.91 ± 9.17 for *D. vulgaris* and 8.82 ± 8.34 for *D. balticum*).

XANES and EXAFS results

The XANES and EXAFS spectra of our FeMoS samples indicate that the oxidation state and first-shell coordination of Mo remained largely unchanged across all conditions tested (Fig. 5). The XANES LCF results indicate that the average Mo oxidation state for the time series samples is 4.37 ± 0.07 and 4.21 ± 0.14 for those formed in uninoculated and inoculated SRB cultures, respectively (Table 1; Table S6). There is a potential decrease in the Mo oxidation state with increasing experimental duration (from ~4.38 to ~4.25 in uninoculated *D. vulgaris* media and from ~4.34 to ~4.00 in inoculated *D. vulgaris* cultures), but this decrease is not consistent across all time series samples and the magnitude of change is not sufficient to rule out analytical variation as the cause (Fig. 3a). Overall, no significant changes or trends in Mo oxidation state were observed with changes in experimental duration, initial ratio of Fe:Mo, degree of Mo thiolation in solution, the presence/absence of SRB or SRB species (Fig. 3, Table 1).

Model fits for the EXAFS spectra suggest that the Mo in these FeMoS precipitates is bonded to 4 – 5 S atoms at 2.31 – 2.51 Å (Fig. 5). The best fits for most samples were obtained with 4 S atoms at an average of 2.40 ± 0.01 Å, 1 O atom at 1.65 ± 0.01 Å and 1 Fe atom at 2.88 ± 0.06 Å (Tables 2, S7 and S8). Note that, while the presence of Mo–O and Mo–Fe bonds in the model slightly improves the fit in many cases, they are not necessary to fit the spectra within reasonable chi-squared and R-factor values. Thus, these data cannot confirm the presence or absence of O or Fe in the coordination environment of Mo in these FeMoS complexes. Alternative fits for time series samples and their associated R factors are listed in Table S8 to clarify the differences between including and excluding Mo–O and Mo–Fe bonds in the fits.

Although aqueous Mo speciation was continuously changing as Mo thiolation proceeded over the course of ageing (Fig. S1), the best fits for the time series EXAFS spectra indicate that the Mo–S bond lengths do not increase or decrease significantly with increasing experimental duration (Fig. 6a). The lengths of Mo–S bonds appear to increase (from 2.39 to 2.42 Å) with increasing initial Fe:Mo ratio (from 0.5 to 2) in samples formed in uninoculated and inoculated *D. vulgaris* media (Fig. 6b). However, this trend in Mo–S bond lengths could also be due to natural variation in the bulk analyses of amorphous FeMoS samples or in the fits. Moreover, there is no apparent correlation between Mo–S bond length and the average Mo oxidation state in the precipitate (Fig. 6c). Overall, the Mo–S bond lengths of FeMoS samples formed in abiotic and uninoculated solutions (2.41 ± 0.01 Å) are indistinguishable from those formed in the presence of SRB cells (2.40 ± 0.01 Å).

The only sample markedly different from the rest with regards to its XANES and EXAFS spectra is the abiotic FeMoS precipitate prepared at high pH (~11) (Fig. 5). The XANES spectrum for this sample exhibits a distinct pre-edge feature similar to that present in the molybdate spectrum. XANES LCF indicates that Mo in this sample is of +6 oxidation state (Table 2). EXAFS fitting suggests Mo

https://doi.org/10.1180/gbi.2024.7 Published online by Cambridge University Press

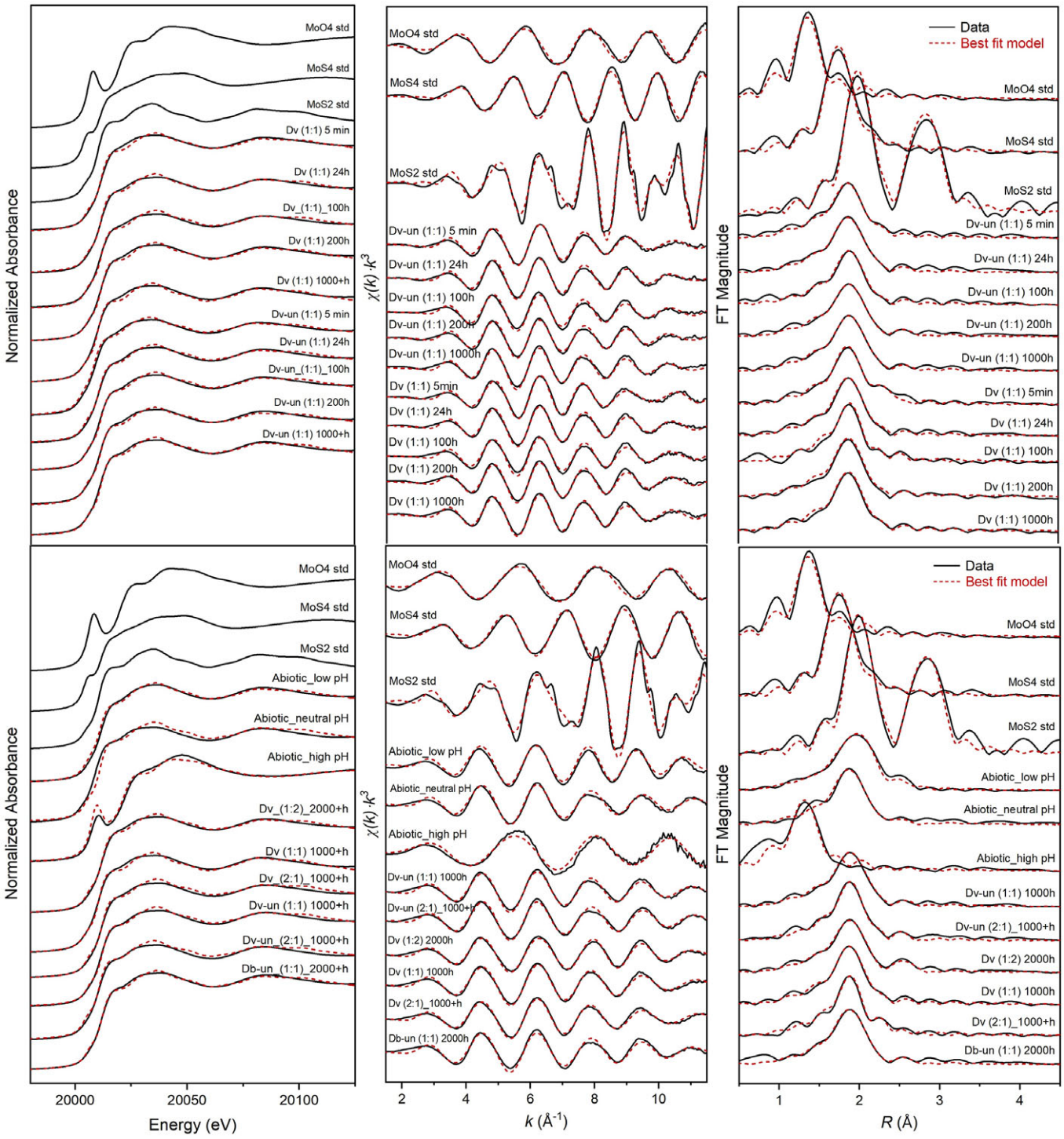

Figure 5. Mo XANES (left), k3 weighed EXAFS spectra (centre), and FT of EXAFS spectra (right) for time series data set (top; listed numerically in Table S8) and abiotic and Fe concentration series data sets (bottom; listed numerically in Table S7). Solid black lines represent data; dashed red lines represent best fit models for each spectra.

coordination in this sample is very similar to that in molybdate, with 4 O atoms at 1.75 ± 0.01 Å (Table 2). This drastic change in Mo oxidation state and coordination was only observed at the high pH (~11) in which this sample was prepared, while the transition from low pH (~4.5) to circumneutral pH (~7.5) did not seem to have a strong effect on the final precipitate. Samples prepared at low and circumneutral pH were similar in Mo oxidation state (4.50 ± 0.18 and 4.36 ± 0.23, respectively) and coordination (1 O atom at ~1.63 – 1.65 Å, 4 S atoms at ~4.32 – 2.50 Å and 1 Fe atom at ~2.88 – 3.00 Å), based on XANES and EXAFS spectra (Fig. 5, Tables S6 and S7).

Discussion

Effect of molybdate and thiomolybdate on SRB growth

The observed inhibition of SRB growth in the presence of MoO_4^{2-} is consistent with previous understanding that molybdate is toxic toward SRB due to its structural similarities to SO_4^{2-}, which allows molybdate to bind with sulfate transporters and subsequently enter the metabolic path for sulfate reduction (*e.g.*, Chen et al., 1998; Biswas et al., 2009; Stoeva and Coates, 2019). Our findings suggest that *D. vulgaris* growth is potentially more strongly

https://doi.org/10.1180/gbi.2024.7 Published online by Cambridge University Press

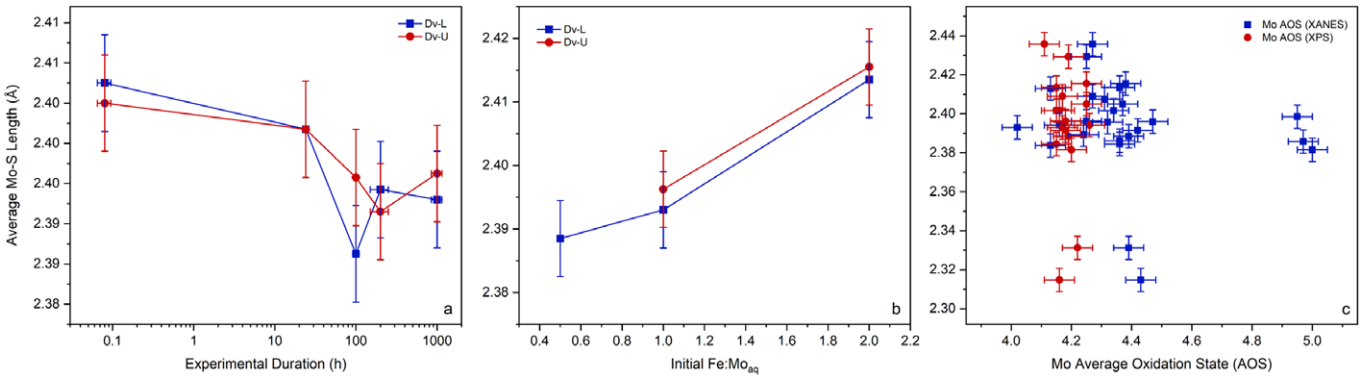

Figure 6. Average Mo–S interatomic distances (based on EXAFS best fits) over experimental duration (a), initial Fe:Mo ratios (b), and average precipitate Mo oxidation state (c). Oxidation state data presented here excludes the high pH sample, containing oxidized Mo(VI).

Table 2. The average EXAFS fit for our FeMoS precipitates compared to EXAFS data from both field and experimental samples reported in previous studies. This table is modified from Table 1 in Helz and Vorlicek (2019) and Table 7 in Dahl et al. (2013).

Sample	N	R_O (Å)	N	R_{S1} (Å)	N	R_{S2} (Å)	N	R_{S3} (Å)	N	R_{Fe} (Å)	Mo Ox.	Reference
Standards												*This study*
MoO_4^{2-}	4	1.77									6	
MoS_4^{2-}			4	2.17							6	
MoS_2			6	2.39					6	3.15[c]	4	
Samples												*This study*
Abiotic $FeMo^{IV}S$[a]	1	1.63–1.69	1	2.31–2.35	1	2.35–2.42	2	2.45–2.51	1	2.88–2.99	4.3–4.5	
Biotic $FeMo^{IV}S$[b]	1	1.65	1	2.31–2.33	1	2.34–2.36	2	2.44–2.49	1	2.71–2.95	4.0–4.4	
High pH $Mo^{VI}O_4^{2-}$	4	1.75									6	
Sediment												*Previous studies*
Black Shales	2–3	1.69–1.71	1–2	2.31–2.38					1	2.60–2.64	4–6	Helz et al. (1996)
Western interior seaway	2.4	1.70	1.6	2.37							4.7–5.3	Tessin et al. (2019)
Anoxic mud (Lake Cadagno)- Type S	0–2	1.94–2.14	4	2.24–2.38					1	2.71–2.73	4.2	Dahl et al. (2013; 2017)
Anoxic mud (Lake Cadagno)- Type OS	1	1.69–1.74	1	2.38	1	2.42	2	2.45	1	2.73–2.77	5.9	Dahl et al. (2013; 2017)
Experimental precipitates												*Previous studies*
$Fe^{IV}MoS_2(S_2)$			2	2.30–2.32	3	2.44–2.47			1	2.79–2.81	4.0–4.1	Vorlicek et al. (2018)
$Mo^{IV}O(S_4)^{2-}$	1	1.69	4	2.38							4	Draganjac et al. (1982)
$Mo_2^{V}O_2S_2\ (S_2)^{2-}$	2	1.68	2	2.11	2	2.32	4	2.41			5	Clegg et al. (1980)
$Mo_2^{V}S_4(S_2)_2^{2-}$			2	2.12	2	2.31	4	2.39			5	Pan et al. (1984)
$Mo_2^{V}(S_2)_6^{2-}$			2	2.42	4	2.49					5	Müller et al. (1978)
MoS_3			6	2.43					1	2.6–2.9[c]	4	Hibble et al. (1995)
MoS_4^{2-}/FeS_2 absorbate	0.1–4	1.76–1.78	0–4	2.39–2.41					0–3	2.68–2.72[c]		Bostick et al. (2003)
MoS_4^{2-}/FeS_2 absorbate			4	2.43					1	2.99	4	Freund et al. (2016)
MoS_4^{2-}/2MPA/FeS_2 absorbate	1	2.19	6	2.43					1	3.03	4	Freund et al. (2016)
MoO_4^{2-}/FeS_2 absorbate	4	1.75 ± 0.01							1	2.88 ± 0.01	5.5	Freund et al. (2016)

(*Continued*)

https://doi.org/10.1180/gbi.2024.7 Published online by Cambridge University Press

Table 2. (*Continued*)

Sample	N	R_O (Å)	N	R_{S1} (Å)	N	R_{S2} (Å)	N	R_{S3} (Å)	N	R_{Fe} (Å)	Mo Ox.	Reference
Fe-Mo-S-humate (pH 7)	2	1.68	2	2.31								Helz et al. (1996)
Fe-Mo cubane (*C. pasteurianum*)			3–4	2.35 ± 0.03	1–2	2.49 ± 0.03			1	2.72 ± 0.05	4	Cramer et al. (1978); Venters et al. (1986)
DMSO reductase	1	1.72	1	2.38	1	2.42	2	2.45			4	Dias (1999; Dahl et al. (2017)
Live SRB-associated MoS precipitates	1	1.73	1	2.34	1	2.36	2	2.40 ± 0.01			4.8	Dahl et al. (2017)
Dead SRB-associated MoS precipitates	1	1.69 ± 0.07	4	2.35 ± 0.06							4.8–5.2	Dahl et al. (2017)
Dead SRB-associated MoS precipitates	1	1.66 ± 0.07	5	2.37 ± 0.04							4.0–4.4	Dahl et al. (2017)

[a]Range of interatomic distances for best fits of $FeMo^{IV}S$ precipitates formed in abiotic solutions or uninoculated culture media.
[b]Range of interatomic distances for best fits of $FeMo^{IV}S$ precipitates formed in biological solutions (SRB cultures).
[c]Mo–Mo in molybdenite (MoS_2)

inhibited by MoO_4^{2-} than *D. balticum* growth (Fig. S1). The different responses to MoO_4^{2-} exhibited by the two species may be due to differences in the specificity and sensitivity of their sulfate transporters such that those in *D. vulgaris* do not as easily distinguish between MoO_4^{2-} and SO_4^{2-}, thus transferring more MoO_4^{2-} into their cells, leading to more severe inhibition (Stoeva and Coates, 2019). Alternatively, because the *D. balticum* media contains higher concentrations of Ca^{2+} and Mg^{2+}, which may form strong ion-pairs with MoO_4^{2-}, this lowers the activity and, thus, the toxicity of MoO_4^{2-} in this media, potentially explaining the weaker inhibition of *D. balticum* growth compared to *D. vulgaris* (Helz et al., 2011).

The effect of thiomolybdate on SRB had not been previously tested by direct addition of MoS_4^{2-} to SRB cultures (only by MoO_4^{2-} addition, which inhibits sulfide production and, thus, does not allow the full conversion of MoO_4^{2-} to MoS_4^{2-}). Our results suggest that MoS_4^{2-} also inhibits bacterial sulfate reduction, potentially more strongly than MoO_4^{2-} (Fig. S1). However, a quantitative comparison of the degree of inhibition caused by MoO_4^{2-} versus MoS_4^{2-} is difficult as the solution turbidity and sulfide concentration measurements used to estimate SRB growth are altered by the presence of MoS_4^{2-}.

Since both MoO_4^{2-} and MoS_4^{2-} effectively inhibit SRB growth at relatively low concentrations, these compounds are probably transported into SRB cells through sulfate transporters (Nair et al., 2015; Stoeva and Coates, 2019). However, given the lack of Mo precipitation in Mo-containing cultures, this uptake is probably not a major sequestration pathway in natural euxinic environments and is also not permanent due to the lack of Mo reduction associated with this uptake (Stoeva and Coates, 2019; Phillips and Xu, 2021).

Mo thiolation in abiotic and biotic systems

Full conversion of MoO_4^{2-} to MoS_4^{2-} was achieved in all biological systems tested as seen in abiotic systems at low to circumneutral pH, suggesting that the presence of live *D. vulgaris* or *D. balticum* cells does not limit the degree of Mo thiolation under these conditions. The faster rate of Mo thiolation in *D. vulgaris* media (both inoculated and uninoculated) compared to that in *D. balticum* media is potentially due to their slight differences in pH (initial pH of *D. vulgaris* media = 7.76 ± 0.16; initial pH of *D. balticum* media = 7.01 ± 0.17) (*e.g.*, Lohmayer et al., 2015; Vorlicek et al., 2015; Phillips et al., 2023). The differences in ionic strength of *D. vulgaris* media (~0.1 M) relative to *D. balticum* media (~0.7 M) may have also played a role as more rapid flocculation of FeS precipitates in *D. balticum* media may reduce the availability of reactive surface sites, where the replacement of O atoms in MoO_4^{2-} with S atoms is catalysed. However, given that faster Mo thiolation in *D. vulgaris* media relative to *D. balticum* media was observed in both the presence and absence of Fe^{2+}, pH was probably the major factor.

The faster rate of Mo thiolation and sequestration in live *D. vulgaris* cell cultures compared to uninoculated media (Figs 1 and S2) is potentially due to the presence of (1) cell surfaces that act as catalytic sites, (2) activated sulfur species (*i.e.*, intermediates of bacterial sulfate reduction) and/or (3) microenvironments with higher concentrations of sulfide. It is possible that SRB cell surfaces adsorb MoO_4^{2-} and facilitate reactions of molybdate and sulfide/other reduced sulfur species. However, our experimental results show that Mo reduction requires Fe^{2+} in all live cell-containing cultures, thus the proposed role of SRB in facilitating Mo–S redox reactions is probably only significant in the presence of iron. Moreover, given the similar rates of Mo thiolation observed in live *D. balticum* cell cultures compared to uninoculated *D. balticum* media, it is unlikely that SRB cells catalyse Mo thiolation to a degree that would heavily alter Mo behaviour in nature. Alternatively, higher polysulfide concentrations in live cultures (as indicated by the more intense UV-vis peak at ~345 nm) compared to uninoculated cultures may have increased Mo thiolation and sequestration rates, as polysulfide has been previously proposed to induce Mo reduction (Vorlicek et al., 2004; Helz and Adelson, 2013; Freund et al., 2016; Vorlicek et al., 2018).

Mo reduction in abiotic and biotic systems

All FeMoS precipitates formed at low to circumneutral pH (~4.3 to 8.0) contain predominantly reduced Mo(IV) (Table 1). Only the FeMoS precipitates formed at high pH (~11.0) contain predominantly oxidized Mo(VI), probably due to the lack of Mo thiolation in high pH systems (*e.g.*, Phillips et al., 2023). Because Mo thiolation and reduction were not observed in high pH experiments, only the results from low to circumneutral pH systems are discussed for the remainder of this section.

https://doi.org/10.1180/gbi.2024.7 Published online by Cambridge University Press

The high-resolution XPS fitting and XANES LCF results are in close agreement with average Mo oxidation states of 4.18 ± 0.04 and 4.24 ± 0.18 for abiotic and biotic samples, respectively, based on the XPS data and 4.31 ± 0.06 and 4.34 ± 0.24 for abiotic and biotic samples, respectively, based on the XANES data (Table 1). Given the consistent Fe^{2+} requirement across abiotic and biotic samples for Mo reduction and precipitation as well as the similar average Mo oxidation states in abiotic and biotic precipitates, it is unlikely that SRB directly affected Mo reduction in these experiments. The more intriguing trend in the Mo oxidation state data is the positive correlation observed between the relative amounts of reduced Mo (IV) and Fe (II) (Fig. 4a). This trend highlights the close relationship between Fe coordination (reflected in its valence) and Mo reduction in these Fe–Mo–S systems. Although we cannot completely rule out the observed Fe(II)-Mo(IV) correlation (Fig. 4a) as an artefact of sample oxidation during analysis, this possibility is minimal given that the samples were prepared in an anaerobic chamber (N_2:H_2 = 97%:3%) and transported in anaerobic serum vials stored in airtight Thermo Scientific AnaeroPack containers with oxygen scavengers; sample surfaces were sputtered during XPS analyses to remove any of the surface material that may have become partially oxidized. That said, another more likely explanation for the observed Fe(II)-Mo (IV) correlation is that the reactivity of Fe in the precursors and initial precipitate is highly dependent on its structural position; those that are able to fit into a centre position of S polyhedra (*i.e.*, of lower reactivity) are exclusively Fe(III) due to size limitations, resulting in a positive relationship between Mo reduction and Fe(II). However, further experiments are needed to verify this hypothesis.

The slight decrease in the average Mo oxidation state and the increase in the overall amount of Mo sequestered with increasing experimental duration (Figs 3a and 2b, respectively) indicate a potential relationship between Mo sequestration and reduction (Fig. 3b). However, the trends in the data are insufficient to rule out analytical or natural variation and there is no observable trend in average Mo oxidation state with S concentration in the precipitates (Fig. 4c) despite the positive relationship between Mo and S concentration in the final precipitates (Fig. 2d). This suggests that the amount of overall sulfide precipitation and, thus, Mo sequestration does not significantly affect the degree of Mo reduction in the resulting precipitate.

Role of iron (Fe)

The faster Mo thiolation and sequestration rates in the presence of Fe^{2+} observed in all experimental systems (Figs 1 and 2), suggests that Fe^{2+} catalyses these processes as found in previous studies (Bonomi et al., 1992; Helz et al., 2004; Phillips et al., 2023). Moreover, the requirement of Fe^{2+} for Mo sequestration in experimental conditions emphasizes the importance of Fe^{2+} for Mo sequestration. Although only present at trace concentrations, slight variations in Fe^{2+} concentrations in natural basins may be partially responsible for the variations in Mo behaviour observed across modern euxinic basins (Helz, 2021; Phillips et al., 2023).

The degree to which Fe^{2+} addition catalysed Mo thiolation and sequestration in our experiments did not scale consistently with increasing the initial Fe^{2+} concentration, suggesting that at lower Fe^{2+} concentrations, like those present in natural settings, the catalysis effect of Fe^{2+} may be just as strong. For example, the occurrence of precipitation in our 'Fe-free' SRB cultures (in contrast to the lack of precipitation in Fe-free uninoculated media), suggests either that (1) these cells provide reactive surfaces that induce Mo reduction and precipitation in the absence of Fe^{2+} or (2) trace amounts of Fe^{2+} were unintentionally transferred into the media during inoculation from a previous (Fe-containing) culture. Given that the ICP-OES and XPS data revealed the presence of Fe^{2+} in these solutions and precipitates (Table S4), it is likely that the presence of trace Fe^{2+} led to the Mo sequestration observed in these samples.

The concentration of transferred Fe^{2+} in these solutions was only ~0.002 – 0.026 mM, based on the concentration that could have been transferred from the 1% inoculation of the original Fe-containing culture (Table 1). Because Mo precipitation occurs at such low Fe^{2+} concentrations, comparable to those observed in some modern euxinic basins (*e.g.*, Emerson and Huested, 1991; Helz et al., 2011; Nägler et al., 2011; Dellwig et al., 2019), it is likely that this Fe catalytic effect on Mo thiolation and sequestration also operates in natural euxinic settings. Here we also argue that previously reported 'Fe-independent' removal of Mo facilitated by SRB (*e.g.*, Dahl et al., 2017) involved similar Fe-catalysation as the media used contained Fe (at ~0.026 mM), which, based on our findings, is sufficient to facilitate Mo precipitation. Future work should investigate the influence of other redox-active trace metal cations, such as nickel and copper, on Mo behaviour in euxinic conditions. These metals may exhibit similar catalytic behaviour to iron, potentially enabling Fe-independent pathways of Mo sequestration.

Role of sulfate-reducing bacteria (SRB)

Comparison between the two SRB species utilized in this study yields major differences in the estimated thiolation and sequestration rates (Fig. 1), but these differences are present in uninoculated controls as well. Thus, the faster Mo thiolation and sequestration observed in uninoculated and inoculated *D. vulgaris* cultures compared to those of *D. balticum* cultures is due to abiotic factors, such as the higher initial pH and ionic strength of *D. balticum* media (7.76 ± 0.16 and ~0.7 M) compared to *D. vulgaris* media (7.01 ± 0.17 and ~0.1 M). The presence of the SRB cells was shown to have relatively minor effects on Mo thiolation and sequestration.

In all circumneutral to high pH (~7 – 11) experiments, Fe was required for Mo sequestration in either the presence or absence of the SRB cells. The absence of precipitation in cultures lacking Fe suggests that the SRB cells and other OM present in the cell cultures cannot directly induce Mo reduction and sequestration without Fe (Table S2). Furthermore, no major differences are observed in the Mo oxidation state and coordination environment in the precipitates formed in the presence of *D. vulgaris/D. balticum* cells compared to those formed abiotically. Thus, although previous studies have suggested that SRB may actively induce Mo sequestration (*e.g.*, by taking up and reducing MoO_4^{2-}; Biswas, et al., 2009), the results of this study indicate that the role SRB plays in Mo sequestration is passive (*i.e.*, by providing the sulfide with which Mo reacts; Helz and Vorlicek, 2019) and relatively minor compared to that of Fe.

Other studies have suggested that even if SRB do not actively take up and reduce Mo, they may act as carriers of Mo to the sediment by providing reactive cell surfaces that adsorb, complex and immobilize molybdate (Biswas et al., 2009; Dahl et al., 2017). As described previously, rates of Mo thiolation and sequestration observed in SRB-containing solutions are, in some cases, slightly higher than those observed in SRB-lacking solutions, which could be in part due to the effects of reactive SRB cell surfaces. However, the Fe:Mo ratios observed in the precipitates formed in the presence of SRB cells are roughly the same as those in abiotic precipitates (Tables S3 and S4), emphasizing the minor role of SRB cells in Mo sequestration.

https://doi.org/10.1180/gbi.2024.7 Published online by Cambridge University Press

Bonding environment of FeMoS precipitates

The best fits for the EXAFS spectra of our FeMoS samples indicate that Mo is coordinated by 4 S atoms at an average distance of 2.40 ± 0.01 Å and, potentially, an O atom at 1.65 ± 0.01 Å and Fe atom at 2.88 ± 0.06 Å (Table 2). The presence of O and Fe is not certain as including these bonds in the models only marginally improves the fits. The length of the Mo–S bonds in our FeMoS samples (2.31 – 2.51 Å) are comparable to those observed in previously studied Mo(IV)-sulfide structures, such as $FeMoS_2(S_2)$ experimental precipitates (2.31 – 2.45 Å; Vorlicek et al., 2018), MoS_4^{2-}/FeS_2 adsorbate (2.43 Å; Freund et al., 2016), FeMoS cubane structures (2.36 ± 0.02 Å; Cramer et al., 1978), SRB cell-associated experimental precipitates (2.33 – 2.45 Å; Dahl et al., 2017), Lake Cadagno sediments (2.24 – 2.38 Å; Dahl et al., 2013), black shales (2.31 – 2.38 Å; Helz et al., 1996), $MoO(S_4)_2^{2-}$ experimental precipitates (2.38 Å; Draganjac et al., 1982) and Mo-Fe proteins in nitrogenase enzymes in nitrogen-fixing bacteria, *Azotobacter vinelandii* and *Clostridium pasteurianum* (2.35 – 2.39 Å; Cramer et al., 1978; Chen et al., 1993; Dahl et al., 2013).

The length of potential Mo–O bonds in our samples (1.65 ± 0.01 Å) are shorter than those present in $Mo(VI)O_4^{2-}$ (1.78 Å) and $Mo(VI)O_3$ (1.75 Å) MoS_4^{2-}/FeS_2 adsorbate (1.76 – 2.19 Å) (Bostick et al., 2003; Dahl et al., 2013; Freund et al., 2016, Table 2). They are closer to, but still slightly shorter than, Mo–O bonds found in Lake Cadagno sediment at 1.69 – 1.74 Å (Dahl et al., 2013) and black shales at 1.69 – 1.71 Å (Helz et al., 1996). They are also comparable to the 1.64 – 1.73 Å Mo–O bonds found in molybdate-OM complexes (where OM is oxalate, malate, citrate, catecholate or tannic acid; Wagner et al., 2017). However, these molybdate-OM complexes contain oxidized Mo(VI) in contrast to our samples that contain reduced Mo(IV).

Given the short Mo–O interatomic distances, these may represent terminal Mo=O bonds (Table 2). Previous studies show that Mo=O bonds typically result in the presence of a pre-edge feature in the XANES spectra as observed in molybdate spectra (Dahl et al., 2013; 2017; Wagner et al., 2017). However, the absence of this pre-edge feature in most of our samples is probably due to the amorphous nature of our precipitates, as the pre-edge feature is most prominent in minerals with tetrahedral geometry such as molybdate or tetrathiomolybdate (Wagner et al., 2017; Fig. 5). Alternatively, the absence of this pre-edge feature may indicate the absence of Mo–O/Mo=O bonds altogether as, in most samples, the presence of O in the Mo coordination environment only marginally improves the fit.

The length of potential Mo–Fe bonds in our samples (2.88 ± 0.06 Å) are comparable to those observed in Lake Cadagno sediments (2.85 – 2.96 Å; Dahl et al., 2013) and $FeMoS_2(S_2)$ experimental precipitates (2.79 – 2.81 Å; Vorlicek et al., 2018), but shorter than those observed in MoS_4^{2-}/FeS_2 adsorbate (2.99 – 3.03 Å; Freund et al., 2016) and longer than those observed in black shales (2.60 – 2.64 Å; Helz et al., 1996), FeMoS cubane structures (2.72 ± 0.03 Å; Cramer et al., 1978) and Mo-Fe proteins in nitrogenase enzymes in nitrogen-fixing bacteria, *Azotobacter vinelandii* and *Clostridium pasteurianum* (2.69 – 2.70 Å Cramer et al., 1978; Chen et al., 1993; Dahl et al., 2013; Table 2). Such comparisons may help confirm the mechanisms involved in Mo sequestration in euxinic basins. For example, the modelled Mo-S, Mo-O and Mo-Fe bonds in our precipitates indicate Mo species similar in coordination to those found in Lake Cadagno sediments, suggesting similar abiotic formation processes.

The XANES and EXAFS spectra of most of our FeMoS samples are largely the same, with only minor differences (Fig. 5). However, the Mo present in the FeMoS precipitates formed under high pH (~11.0) conditions are fundamentally different from those formed under low to circumneutral pH (~4.3 – 8.0). The high pH precipitates exhibit Mo XANES and EXAFS spectra comparable to that of $Mo(VI)O_4^{2-}$, suggesting that the molybdate initially added to these solutions may have adsorbed to the FeS colloids/precipitates without undergoing reduction and coprecipitation as FeMoS. Given the much lower concentration of Mo in these precipitates (0.60 ± 0.06 at.%) relative to those formed at low to circumneutral pH (4.94 ± 3.81 at.%), it is likely that the lack of Mo thiolation at such high pH prevents the reductive sequestration of Mo in these systems (*e.g.*, Phillips et al., 2023). Thus, the $Mo(VI)O_4^{2-}$ observed in this sample is probably susceptible to remobilization if resuspended in solution (Kowalski et al., 2013; Ardakani et al., 2016; Dahl et al., 2017). This finding further emphasizes the significance of Mo thiolation and, thus, pH in controlling Mo sequestration under sulfidic conditions.

Potential sequential Mo sequestration mechanism

The passive role of SRB suggests an abiotic, Fe-dependent Mo sequestration mechanism, which can take place by either (1) adsorption of molybdate or thiomolybdate onto solid Fe-sulfides or (2) thiomolybdate reaction with dissolved Fe^{2+}, leading to coprecipitation as FeMoS complexes (Bostick et al., 2003; Freund et al., 2016; Dahl et al., 2013; 2017; Vorlicek et al., 2018, Miller et al., 2020). The increase in precipitate Mo concentrations and decrease in aqueous Mo concentrations with increasing experimental duration (Fig. 2b) indicate an increase in the degree of Mo sequestration over the course of ageing. Moreover, the positive relationships observed between Mo, Fe and S concentrations in both precipitates and solutions (Figs 2c and d) indicate an increase in overall FeMoS precipitation with ageing. These relationships connect the increase in precipitate Mo concentrations over time with that in overall FeMoS coprecipitation rather than cumulative Mo adsorption to previously precipitated Fe-sulfides.

Nevertheless, the coordination environment of Mo in our samples based on EXAFS fitting suggests that both coprecipitation and adsorption mechanisms may be involved in Mo sequestration. The MoO_4^{2-} present in the FeS precipitates formed at high pH (Fig. 5, Table 2) and the apparent independence of Mo speciation in the precipitate relative to that in solution in circumneutral pH systems (*i.e.*, the solid-state Mo species remains constant as the species in solution changes/becomes thiolated; Figs 5 and S1), suggest that the reaction of MoO_4^{2-} with colloidal FeS complexes may be the first step in Mo thiolation and reduction in Fe-containing sulfidic systems (Helz et al., 2004).

The lack of change in Mo coordination in the time series precipitates, which were collected while dissolved Mo speciation was still changing drastically, was initially interpreted to indicate that molybdate and thiomolybdate intermediates can be directly reduced and sequestered and that the Mo thiolation and reduction processes are decoupled. However, the lack of thiolation and reduction in the high pH precipitates suggests otherwise (*i.e.*, at least some degree of Mo thiolation appears to be an important requirement for subsequent Mo reduction). Thus, the lack of change in Mo coordination in the time series precipitates is more likely due to a stepwise mechanism of interaction/adsorption, thiolation and reduction/sequestration. That is, MoO_4^{2-} initially reacts with the FeS clusters/nanostructures, which then induces Mo thiolation and subsequent reduction and precipitation as FeMoS (Fig. 7).

The source of S for effective Mo thiolation in Fe-containing circumneutral pH solution is likely from those associated with Fe in freshly formed FeS clusters or nanostructures. Comparison of the

https://doi.org/10.1180/gbi.2024.7 Published online by Cambridge University Press

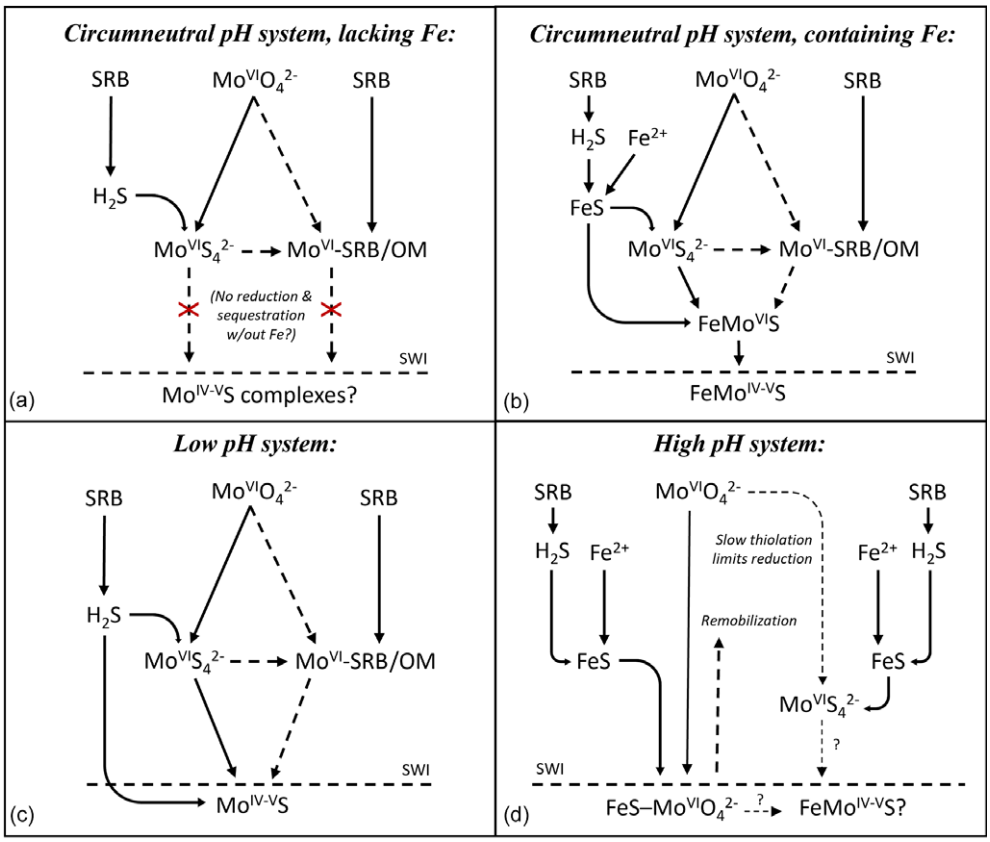

Figure 7 Schematic figure showing the likely pathways of Mo reactions and sequestration in euxinic basins lacking Fe (a), containing Fe (b), with acidic pH (c), and with alkaline pH (d).

Mo thiolation and FeS condensing rates based on calculations using our data and Mo thiolation equilibrium constants (Erickson and Helz, 2000) and formerly reported Fe-S precipitation rate constants (Rickard, 1995) indicates that the formation of FeS complexes/condensed phases precedes Mo thiolation. This FeS-dependent thiolation mechanism of molybdate (under circumneutral pH) may also explain the positive relationships identified among Mo, Fe and S concentrations in the precipitates (Fig. 2d).

The proposed FeS-dependent Mo thiolation is also consistent with the observed lack of Mo thiolation in Fe-containing high pH systems (Fig. 5) as FeS formation kinetics are strongly dependent on pH (*i.e.*, the higher the pH, the faster FeS condenses). As the solution pH increases, the formed FeS probably proceeds far beyond the initial FeS cluster/nanostructure stage, becoming too dense to provide sufficient reactive sites that may catalyse the Mo thiolation. However, in the circumneutral pH systems, the FeS precipitation rate is sufficiently reduced to enable Mo thiolation and subsequent reduction/sequestration.

Given that Fe is required for Mo reduction in circumneutral to high pH systems, even in solutions with other 'nucleation sites' (*e.g.*, SRB cells), Fe probably plays a direct role in facilitating the electron transfer from S to Mo in these systems. However, the Fe-independent Mo sequestration observed in low pH systems indicates that Mo reduction can occur in the absence of Fe and, thus, suggests a different Mo sequestration mechanism altogether (Phillips et al., 2023). We confirmed that Mo thiolation is required for Mo reduction and that a net redox reaction occurs between Mo(VI) and S(-II). Despite the different molecular mechanisms, Mo sequestration in both low pH and Fe-containing, circumneutral pH solutions may occur via the redistribution of electrons in the tetrathiomolybdate structure; thus, it is either low pH or FeS clusters that catalyse this self-redox reaction.

Previous studies have associated an increase in Mo–S bond length with an increase in structural stability of the Mo-sulfide (*e.g.*, Freund et al., 2016; Wagner et al., 2017). However, our EXAFS data show no increase in Mo–S bond length with increasing experimental duration in both inoculated SRB cultures and uninoculated media (Table S8, Fig. 6a), indicating a lack of structural change over the course of the reaction. Moreover, the lack of correlation between Mo–S length and average Mo oxidation state in the precipitate (Fig. 6c) also suggests that the coordination and bulk oxidation state of Mo in the precipitates remained relatively stable, despite the ongoing Mo sequestration and the increase in overall precipitation throughout the course of each experiment. The only factor observed to cause a distinct increase in Mo–S length was an increase in the initial Fe:Mo ratio (*i.e.*, an increase in initial aqueous Fe^{2+} concentration) (Fig. 6b). This suggests that, in addition to its role in catalysing Mo thiolation and reduction, Fe^{2+} may also increase the structural stability of FeMoS precipitates.

Freund et al. (2016) found that Mo–S bonds in FeMoS complexes formed by tetrathiomolybdate adsorption to pyrite were elongated relative to the initial tetrathiomolybdate (2.43 vs 2.19 Å), suggesting structural rearrangement of tetrathiomolybdate upon sorption and reduction. The FeMoS precipitates formed in our experiments exhibit similar Mo–S bond lengths (average = 2.40 ± 0.03 Å), indicating potentially similar final structures. Moreover, Freund et al. (2016) found that when OM was added to solutions containing FeMoS precipitates formed *via* adsorption of

https://doi.org/10.1180/gbi.2024.7 Published online by Cambridge University Press

tetrathiomolybdate to FeS_2, Mo–O bonds were present in the final precipitates due to the reaction between tetrathiomolybdate and the OM to form an OM-Mo-FeS_2 complex (Freund et al., 2016). Thus, the potential presence of Mo–O bonds in our samples based on EXAFS fitting suggests that our FeMoS precipitates may represent similar OM-Mo-FeS structures. However, our FeMoS precipitates appear to have formed via coprecipitation rather than Mo adsorption. Moreover, the S speciation in our precipitates indicates the dominance of monosulfide over disulfide. Thus, the mechanism of Mo sequestration and the sulfur or FeS species that reduce Mo may not strongly alter the resulting Mo coordination in the final precipitate.

Conclusions

Sulfate-reducing bacterial species *D. vulgaris* and *D. balticum* are both inhibited by Mo but have very little effect on Mo behaviour. Although previous studies have suggested that SRB cells and other organic materials may complex Mo in sulfidic solutions and facilitate its sequestration (*e.g.*, Chen et al., 1998; Orberger et al., 2007; Biswas et al., 2009; Dahl et al., 2017), our experiments indicate that SRB cells play a negligible role in Mo sequestration. Thus, results from this study suggest that Mo-OM covariations in euxinic sediment are probably not due to active Mo uptake, reduction or complexation by SRB but, rather, the production of sulfide by SRB which reacts with molybdate to form tetrathiomolybdate, which is then sequestered. This process leads to the misleading correlation between Mo and OM in the rock record, as was suggested by Helz and Vorlicek (2019). Given the two very different SRB species tested in this study exhibited similar effects on molybdate and thiomolybdate behaviour, it is likely that these results also represent the behaviour of other SRB species common in euxinic environments. However, it is important to note there is a wide diversity of SRB species, and those not investigated in this study may interact with Mo differently than *D. vulgaris* or *D. balticum*.

The major factors that appear to control Mo speciation and sequestration in biological systems are the same as those found to control Mo behaviour in abiotic systems: sulfide concentration, pH and Fe^{2+} concentration (*e.g.*, Helz et al., 1996; Phillips et al., 2023). Based on our experiments, Mo precipitation, even in the presence of live or dead SRB cells, relies on the presence of Fe^{2+} under circumneutral pH conditions, suggesting that Mo sequestration is dependent on Fe^{2+} (and/or potentially other transition metals) but not dependent on SRB (only on the sulfide that they produce). The importance of Fe^{2+} in these experimental systems highlights the need for further investigation into the effect of other metal cations on Mo sequestration. An understanding of the factors that control and potentially limit Mo sequestration in natural settings is critical for improving the accuracy and precision of palaeoredox reconstructions.

In addition to Fe^{2+}, pH strongly controls Mo thiolation and subsequent sequestration in both abiotic and biotic solutions. Molybdenum reduction took place in all Fe-containing low to circumneutral pH conditions, for which precipitates contain predominantly Mo(IV) (Table 1). However, in highly alkaline conditions, molybdate did not become thiolated, even in the presence of Fe^{2+} (Fig. 5), suggesting that in natural alkaline conditions, Mo sequestration may become limited with respect to Mo replenishment (Fig. 7), leading to non-quantitative removal and erroneous interpretations of Mo signatures (Phillips et al., 2023). Future experimental work carried out under more environmentally relevant concentrations, followed by further investigation into the aqueous chemistry of modern euxinic basins, like those carried out by Helz (2021, 2022) would provide more insight into the potential limiting factors controlling Mo sequestration in natural settings, which would greatly improve our interpretations of Mo signatures in ancient sediment.

Supplementary material. The supplementary material for this article can be found at http://doi.org/10.1180/gbi.2024.7.

Acknowledgements. This material is based upon work supported by the U.S. Department of Energy, Office of Science, Basic Energy Sciences program under Award Number DE-SC0023251. This work used shared facilities at the Nanoscale Characterization and Fabrication Laboratory, which is funded and managed by Virginia Tech's Institute for Critical Technology and Applied Science. Additional support was provided by the Virginia Tech National Center for Earth and Environmental Nanotechnology Infrastructure (NanoEarth), a member of the National Nanotechnology Coordinated Infrastructure (NNCI), supported by NSF (ECCS 1542100 and ECCS 2025151). Part of the research described in this paper was performed at the Canadian Light Source, a national research facility of the University of Saskatchewan, which is supported by the Canada Foundation for Innovation (CFI), the Natural Sciences and Engineering Research Council (NSERC), the Canadian Institutes of Health Research (CIHR), the Government of Saskatchewan and the University of Saskatchewan.

References

Algeo, T.J. and Lyons, T.W. (2006) Mo–total organic carbon covariation in modern anoxic marine environments: implications for analysis of paleoredox and paleohydrographic conditions. *Paleoceanography* **21**, 1–23.

Ardakani, O.H., Chappaz, A., Sanei, H. and Mayer, B. (2016) Effect of thermal maturity on remobilization of molybdenum in black shales. *Earth Planet. Sci. Lett.*, **449**, 311−320.

Biswas, K.C., Woodards, N.A., Xu, H. and Barton, L.L. (2009) Reduction of molybdate by sulfate-reducing bacteria. *Biometals*, **22**, 131–139.

Bonomi, F., Iametti, S. and Kurtz, D.M. (1992) Acceleration by Fe(II) of thiomolybdate formation from aqueous molybdate and sulfide. A simplified synthesis of $[Fe(MoS_4)_2]^{3-}$. *Inorg. Chim. Acta*, **193**, 125–128.

Bostick, B.C., Fendorf, S. and Helz, G.R. (2003) Differential adsorption of molybdate and tetrathiomolybdate on pyrite (FeS2). *Environ. Sci. Technol.*, **37**, 285–291.

Chandrasekaran, J., Ankara, M.A. and Sarkar, S. (1987) Aging of ammonium tetrathiomolybdate(VI) in air: an example of induced electron transfer be external oxidant, oxygen. *J. Less-common Met.*, **134**, 2, 23–25.

Chappaz, A., Lyons, T.W., Gregory, D.D., Reinhard, B.C., Gill, C. and Large, R.R. (2014) Does pyrite act as an important host for molybdenum in modern and ancient euxinic sediments? *Geochim. Cosmochim. Acta*, **74**, 203–214.

Chen J., Christiansen J., Tittsworth R., Hales B., George S., Coucouvanis D. and Cramer S. (1993) Iron EXAFS of Azotobacter vinelandii nitrogenase Mo-Fe and V-Fe proteins. *J. Am. Chem. Soc.*, **115**, 5509–5515.

Chen, G., Ford, T.E. and Clayton, C.R. (1998) Interaction of sulfate-reducing bacteria with molybdenum dissolved from sputter-deposited molybdenum thin films and pure molybdenum powder. *J. Colloid Interface Sci.*, **204**, 237–246.

Clegg, W., Mohan, N., Müller, A., Neumann, A., Rittner, W. and Sheldrick, G.M. (1980) Crystal and molecular structure of [N(CH3)4]2[Mo2O2S2(S2)]: A compound with two S22− ligands. *Inorg. Chem.*, **19**, 2066–2069.

Cramer S.P., Gillum, W.O., Hodgson, K.O., Mortenson, L.E., Stiefel, E.I., Chisnell, J. R., Brill, W.J. and Shah, V.K. (1978) The molybdenum site of nitrogenase. 2. A comparative study of MO-Fe proteins and the iron-molybdenum cofactor by x-ray absorption spectroscopy. *J. Amer. Chem. Sot.*, **100**, 3814–3819.

Crichton, R. (2019) *Chapter 17- Molybdenum, Tungsten, Vanadium and Chromium*. Biological Inorganic Chemistry, Third edition. A New Introduction to Molecular Structure and Function, pp. 475–498.

Dahl, T.W., Chappaz, A., Fitts, J.P. and Lyons, T.W. (2013) Molybdenum reduction in a sulfidic lake: Evidence from x-ray absorption fine structure spectroscopy and implications for the Mo paleoproxy. *Geochim. Cosmochim. Acta*, **103**, 213–231.

Dahl, T.W., Chappaz, A., Hoek, J., McKenzie, C.J., Svane, S. and Canfield, D.E. (2017) Evidence of molybdenum association with particulate organic matter under sulfidic conditions. *Geobiol.*, **15**, 311–323.

Dellwig, O., Beck, M., Lemke, A., Lunau, M., Kolditz, K., Schnetger, B., and Brumsack, H.J. (2007) Non-conservative behaviour of molybdenum in coastal waters: Coupling geochemical, biological, and sedimentological processes. *Geochim. Cosmochim. Acta*, **71**, 2745–2761.

Dellwig, O., Wegwerth, A., Schnetger, B., Schulz, H. and Arz, H.W. (2019) Dissimilar behaviors of the geochemical twins W and Mo in hypoxic-euxinic marine basins. *Earth Sci. Rev.* **193**, 1–23.

Dias, J.M., Than, M.E., Humm, A., Huber, R., Bourenkov, G.P., Bartunik, H.D., Bursakov, S., Calvete, J., Caldeira, J., Carneiro, C., Moura, J.J.G., Moura, I., and Romão, M.J. (1999) Crystal structure of the first dissimilatory nitrate reductase at 1.9 A solved by MAD methods. *Structure*, **7**, 65–79.

Demtröder, L., Narberhaus, F. and Masepohl, B. (2019) Coordinated regulation of nitrogen fixation and molybdate transport by molybdenum. *Mol.* Microbiol., **111**, 17–30.

Draganjac M., Simhon E., Chan L.T., Kanatzidis M., Baenziger N.C. and Coucouvanis D. (1982) Synthesis, interconversions, and structural characterization of the [(S4)2MoS] [(S4)2MoO]2-, [(S4)2MoS] [(S4)2MoO]2-, (Mo2S10)2-, and (Mo2S12)2- anions. *Inorg. Chem.*, **21**, 3321–3332.

Emerson, S.R. and Huested, S.S. (1991) Ocean anoxia and the concentrations of molybdenum and vanadium in seawater. *Mar. Chem.* **34**, 177–196.

Erickson, B.E. and Helz, G.R. (2000) Molybdenum(VI) speciation in sulfidic waters: stability and lability of thiomolybdates. *Geochim. Cosmochim. Acta*, **64**, 1149–1158.

Freund, C., Wishard, A., Brenner, R.; Sobel, M., Mizelle, J., Kim, A., Meyer, D.A. and Morford, J.A. (2016) The effect of a thiol-containing organic molecule on molybdenum adsorption onto pyrite. *Geochim. Cosmochim. Acta*, **174**, 222−235.

Hale, K.L., McGrath, S.P., Lombi, E., Stack, S.M., Terry, N., Pickering, I.J., George, G.N. and Pilon-Smits, E.A.H. (2001) Molybdenum sequestration in Brassica Species. A Role for Anthocyanins? *Plant Physiol.* **126**, 1391–1402.

Helz, G.R. (2021) Dissolved molybdenum asymptotes in sulfidic waters. *Geochem. Persp. Let.*, **19**, 23–26.

Helz, G.R. (2022) The Re/Mo redox proxy reconsidered. *Geochimica et Cosmochimica Acta*, **317**, 507–522.

Helz, G.R. and Adelson, J.M. (2013) Trace Element Profiles in Sediments as Proxies of Dead Zone History; Rhenium Compared to Molybdenum. *Environ. Sci. Technol.*, **47**, 1257−1264.

Helz, G.R. and Vorlicek, T.P. (2019) Precipitation of molybdenum from euxinic waters and the role of organic matter. *Chem. Geol.*, **509**, 178–193.

Helz, G.R., Miller, C.V., Charnock, J.M., Mosselmans, J. F. W., Pattrick, R. A. D., Garner, C.D. and Vaughan, D.J. (1996). Mechanism of molybdenum removal from the sea and its concentration in black shales: EXAFS evidence. *Geochim. Cosmochim. Acta*, **60**, 3631–3642.

Helz, G.R., Vorlicek, T.P. and Kahn, M.D. (2004) Molybdenum scavenging by iron monosulfide. *Environ. Sci. Technol.*, **38**, 4263–4268.

Helz, G.R., Bura-Naki´c, E., Mikac, N. and Ciglene čki, I. (2011) New model for molybdenum behavior in euxinic waters. *Chem. Geol.*, **284**, 323–332.

Hibble S.J., Rice D.A., Pickup D.M. and Beer M.P. (1995) Mo K-edge EXAFS and S K-edge absorption studies of the amorphous molybdenum sulfides MoS4.7, MoS3, and MoS3.nH2O (n = 2). *Inorg. Chem.*, **34**, 5109–5113.

Hlohowskyj, S.R., Chappaz, A. and Dickson, A.J. (2021) *Molybdenum as a Paleoredox Proxy: Past, Present, and Future (Elements in Geochemical Tracers in Earth System Science)*. Cambridge: Cambridge University Press.

Jonkers, H.M., vander Maarel, M.J.E.C., Gemerden, H.V. and Hansen, T.A. (1996) Dimethylsulfoxide reduction by marine sulfate-reducing bacteria. *FEMS Microbiol. Lett.* **136**, 283–287.

Jørgensen, B.B. and Kasten, S. (2006) Sulfur cycling and methane oxidation, in *Marine Geochemistry*, eds H.D. Schulz and M. Zabel, Pp. 271–309. Berlin: Springer.

Jørgensen, B.B., Findlay, A.J. and Pellerin, A. (2019) The Biogeochemical Sulfur Cycle of Marine Sediments. *Front. Microbiol.*, **10**, 849.

Kowalski, N., Dellwig, O., Beck, M., Grawe, U., Neubert, N., Nagler, T.F., Badewien, T.H., Brumsack, H.J., van Beusekom, J.E.E. and Bottcher, M.E. (2013) Pelagic molybdenum concentration anomalies and the impact of sediment resuspension on the molybdenum budget in two tidal systems of the North Sea. *Geochim. Cosmochim. Acta*, **119**, 198–211.

Lohmayer, R., Reithmaier, G. M. S., Bura-Nakić, E. and Planer-Friedrich, B. (2015) Ion-pair chromatography coupled to inductively coupled plasma-mass spectrometry (IPC- ICP-MS) as a method for thiomolybdate speciation in natural waters. *Anal. Chem.*, **87**, 3388–3395.

Lyons, T.W., Anbar, A.D., Severmann, S., Scott, C. and Gill, B.C. (2009) Tracking euxinia in the ancient ocean: A multiproxy perspective and proterozoic case study. *Annual Review of Earth and Planetary Sciences*, **37**, 507–534.

Mendel, R.R. and Bittner, F. (2006) Cell biology of molybdenum. *Biochim. Biophys. Acta* **1763**, 621.

Miller, N., Dougherty, M., Du, R., Sauers, T., Yan, C., Pines, J.E., Meyers, K.L., Dang, Y.M., Nagle, E., Ni, Z., Pungsrisai, T., Wetherington, M.T., Vorlicek, T. P., Plass, K.E. and Morford, J.L. (2020) Adsorption of Tetrathiomolybdate to Iron Sulfides and Its Impact on Iron Sulfide Transformations. *ACS Earth Space Chem.*, **4**, 2246−2260.

Mohajerin, T.J., Helz, G.R. and Johannesson, K.H. (2016) Tungsten-molybdenum fractionation in estuarine environments. *Geochim. Cosmochim. Acta* **177**, 105–119.

Müller, A., Nolte, W.O. and Krebs, B. (1978) [S2Mo(S2)MoS2]2−, a novel complex containing only S22− ligands and a Mo-Mo bond. *Angew. Chem. Int. Ed. Eng.*, **17**, 279–280.

Nägler, T.F., Neubert, N., Böttcher, M.E., Dellwig, O. and Schnetger, B. (2011) Molybdenum isotope fractionation in pelagic euxinia: evidence from the modern Black and Baltic Seas. *Chem. Geol.* **289**, 1–11.

Nair, R.R., Silveira, C.M., Diniz, M.S., and Rivas, M.G. 2015. Changes in metabolic pathways of desulfovibrio alaskensis G20 cells induced by molybdate excess. *J. Biol. Inorg. Chem.*, **20**, 311–322.

Orberger, B., Vymazalova, A., Wagner, C., Fialin, M., Gallien, J.P., Wirth, R., Pasava, J. and Montagnac, G. (2007) Biogenic origin of intergrown Mo-sulphide- and carbonaceous matter in Lower Cambrian black shales (Zunyi Formation, southern China). *Chem. Geol.*, **238**, 213−231.

Pan, W.-H., Harmer, M.A., Halbert, T.R. and Stiefel, E.I. (1984) Induced internal redox processes in molybdenum-sulfur chemistry: Conversion of MoS4- to Mo2S82- by organic disulfides. *Journal of the American Chemical Society*, **106**, 459–460.

Phillips, R.F. and Xu, J. (2021) A critical review of molybdenum sequestration mechanisms under euxinic conditions: Implications for the precision of molybdenum paleoredox proxies. *Earth Sci. Rev.*, **221**, 103799.

Phillips, R.F., Singerling, S., Leng, W. and Xu, J. (2023) Significance of pH and iron-sulfur chemistry for molybdenum sequestration under sulfidic conditions. *Chemical Geology*, **638**, 121702.

Rickard, D. (1995) Kinetics of FeS precipitation: Part 1. Competing reaction mechanisms. *Geochimica et Cosmochimica Acta*, **59**, 21, 4367–4379.

Scott, C., Slack, J.F. and Kelley, K.D. (2017) The hyper-enrichment of V and Zn in black shales of the Late Devonian-Early Mississippian Bakken Formation (USA), *Chemical Geology*, **452**, 24–33.

Stoeva, M.K. and Coates, J.D. (2019) Specific inhibitors of respiratory sulfate reduction: towards a mechanistic understanding. *Microbiology*, **165**, 254–269.

Tessin, A., Chappaz, A., Hendy, I. and Sheldon, N. (2019) Molybdenum speciation as a paleo-redox proxy: A case study from late cretaceous Western Interior Seaway black shales. *Geology*, **47**, 59–62.

Tribovillard, N., Riboulleau, A., Lyons, T. and Baudin, F. (2004) Enhanced trapping of molybdenum by sulfurized marine organic of marine origin in Mesozoic limestones and shales. *Chem. Geol.* **213**, 385–401.

Tucker, M.D., Barton, L.L. and Thomson, B.M. (1997) Reduction and Immobilization of Molybdenum by Desulfovibrio desulfuricans. *J. Environ. Qual.* **26**, 1146–1152.

Tucker, M.D., Barton, L.L. and Thomson, B.M. (1998) Reduction of Cr, Mo, Se and U by Desulfovibrio desulfuricans immobilized in polyacrylamide gels. *J. Ind.Microbiol. Biotechnol.* **20**, 13–19.

Venters, R.A., Nelson, M.J., Mclean, P.A., True, A.E., Levy, M.A., Hoffman, B.M. and Orme-Johnson, W.H. (1986) ENDOR of the resting state of nitrogenase molybdenum- iron proteins from Azotobacter vinelandii, Klebsiella pneumoniae, and Clostridium pasteurianum. Proton, iron- 57, molybdenum-95, and sulfur- 33 studies. *Journal of the American Chemical Society*, **108**, 3487–3498.

https://doi.org/10.1180/gbi.2024.7 Published online by Cambridge University Press

Vorlicek, T.P., Kahn, M.D., Kasuya, Y. and Helz, G. R (2004) Capture of molybdenum in pyrite-forming sediments: Role of ligand-induced reduction by polysulfides. *Geochim. Cosmochim. Acta*, **68**, 547–556.

Vorlicek, T.P., Chappaz, A., Groskreutz, L. M, Young, N. and Lyons, T.W. (2015) A new analytical approach to determining Mo and Re speciation in sulfidic waters. *Chem. Geol.*, **403**, 52–57.

Vorlicek, T.P., Helz, G.R., Chappaz, A., Vue, P., Vezina, A. and Hunter, W. (2018) Molybdenum burial mechanism in sulfidic sediments: iron-sulfide pathway. *ACS Earth Space Chem.*, **2**, 565–576.

Wagner, M., Chappaz, A. and Lyons, T.W. (2017) Molybdenum speciation and burial pathway in weakly sulfidic environments: Insights from XAFS. *Geochim. Cosmochim. Acta*, **206**, 18–29.

Wichard, T., Mishra, B., Myneni, S.C.B., Bellenger, J.P. and Kraepiel, A.M.L. (2009) Storage and bioavailability of molybdenum in soils increased by organic matter complexation. *Nat. Geosci.*, **2**, 625–629.

Xu, J., Murayama, M., Roco, C.M., Veeramani, H., Michel, F.M., Rimstidt, J.D., Winkler, C., and Hochella, M.F. (2016) Highly-defective nanocrystals of ZnS formed via dissimilatory bacterial sulfate reduction: A comparative study with their abiogenic analogues. *Geochimica et Cosmochimica Acta*, **180**, 1–14.

https://doi.org/10.1180/gbi.2024.7 Published online by Cambridge University Press